




**FACULTY OF SCIENCE AND TECHNOLOGY**

**MASTER THESIS**

Study programme / specialisation: Marine and Offshore Technology	The spring semester, 2022 Open / Confidential
Author: Vegard Risa Reisæter	 ..... (signature author)
Course coordinator: Professor Yihan Xing Supervisor(s): Assoc. Prof. Charlotte Obhrai	
Thesis title: Accurate predictions of the Ultimate Limit State Wave Loads on Bottom Fixed Wind Turbine.	
Credits (ECTS): 30	
Keywords: Breaking wave, Pressure Impulse Model, Wave load, Monopile, Ultimate Limit State	Pages: .....48..... + appendix: .....6..... Stavanger, .....15 <sup>th</sup> of June 2022..... date/year

## Abstract

In this project the breaking wave loads on a bottom fixed monopile has been determined with the use of the Pressure Impulse Model. The pressure impulse model is the integral of pressure dependent by time during a short period of time scale. The model was derived for an idealized wave on a vertical cylinder with the variables being crest length, impact height and the free maximum angle of impact which is tuned to give the correct impulse force. Further, the breaking wave loads on a vertical cylinder is determined by using guidelines provided in Det Norske Veritas (DNVGL) and International Electrotechnical Commission (IEC) standards, conditioned on the same sea state applied for the pressure impulse model. The results obtained from the guidelines in DNVGL and IEC standards is compared to the results from the pressure impulse model, and the results obtained shows that the force impulse determined based on these models are overpredicted compared to the pressure impulse model.

## **Acknowledgement**

I would like to thank my supervisor Assoc. Prof. Charlotte Obhrai for her contribution and efforts in the process of completing this thesis. I am grateful for her help and valuable guidance during our meetings.

I also want to thank my co-students for the valuable working environment during this writing process.

# Table of Contents

ABSTRACT .....	2
ACKNOWLEDGEMENT .....	3
LIST OF FIGURES .....	5
1 INTRODUCTION.....	7
1.1 BACKGROUND .....	7
1.2 OBJECTIVES.....	9
1.3 STRUCTURE OF THIS PAPER.....	10
2 BACKGROUND.....	11
2.1 THEORETICAL MODELS .....	11
2.2 NUMERICAL SIMULATIONS.....	12
2.3 EXPERIMENTAL MODELS.....	13
2.4 PRESSURE IMPULSE MODEL .....	14
2.5 DNVGL AND IEC STANDARDS.....	15
2.5.1 IEC 61400-3.....	15
2.5.2 DNVGL-RP-C205, DNVGL-ST-0437 and DNV-OS-J101 .....	16
3 MATHEMATICAL FORMULATION .....	17
3.1 DEFINITION OF BREAKING WAVES .....	17
3.2 INERTIA AND DRAG FORCE .....	18
3.2.1 <i>Definition of Drag and Inertia Coefficient</i> .....	21
3.3 SLAMMING FORCE.....	23
3.3.1 <i>Wagner and von Karman`s Theory</i> .....	24
3.3.2 <i>IEC Standard - Wienke and Oumeraci`s Model</i> .....	25
3.3.3 <i>DNVGL Standard - Campbell and Weynberg`s Model</i> .....	27
3.4 PRESSURE IMPULSE METHOD .....	29
4 RESULTS AND ANALYSIS .....	34
4.1 MATLAB RESULTS .....	34
4.2 DNVGL & IEC STANDARDS .....	40
4.2.1 <i>Drag and Inertia Force Time Histories</i> .....	40
4.2.2 <i>Slam Coefficients Time Histories</i> .....	43
4.2.3 <i>Impact Force Time Histories</i> .....	44
5 DISCUSSION .....	46
6 CONCLUSION .....	46
REFERENCES.....	47
APPENDIX.....	49

## List of Figures

Figure 1.1 Share of substructure types (WindEurope & ETIPWind, 2021) .....	7
Figure 1.2 Monopile structural foundation (Leite, 2015).....	8
Figure 2.1 Inline force comparison (Chella et al., 2016) .....	11
Figure 3.1 Drag coefficient for fixed circular cylinder for steady flow in critical flow regime, for various roughnesses (DNVGL-RP-C205, 2017) .....	21
Figure 3.2 Mass coefficient as function of KC number for smooth (Solid line) and rough (Dotted line) cylinder (DNVGL-RP-C205, 2017) .....	22
Figure 3.3: Nature of the slamming force (Chella et al., 2012) .....	24
Figure 3.4: Von Karman`s formulation (Wienke & Oumeraci 2005).....	24
Figure 3.5: Wagner`s formulation (Wienke & Oumeraci, 2005).....	25
Figure 3.6: Impact force on circular cylinder (Wienke & Oumeraci, 2005).....	26
Figure 3.7 Area exposed to shock pressure (DNVGL-RP-C205, 2017).....	28
Figure 3.8 Definition sketch for 3D block impact on a vertical wall. (Ghadirian & Bredmose, 2019).....	29
Figure 3.9 Definition sketch for axisymmetric impact on a vertical cylinder. (Ghadirian & Bredmose, 2019) .....	30
Figure 3.10: Definition sketch for wedge-shaped 3D impact on a vertical cylinder. (Ghadirian & Bredmose, 2019) .....	32
Figure 4.1: Dimensionless pressure impulse on the cylinder plotted as a function of $z/H$ , at $\theta = 0$ , for several values of $a/b$ .....	35
Figure 4.2: Dimensionless pressure impulse on the inner cylinder, at $\theta = 0$ , plotted as a function of $z/H$ for several values of $b/H$ .....	36
Figure 4.3: Dimensionless pressure impulse on the inner cylinder, at $\theta = 0$ , plotted as a function of $z/H$ for several values of $\mu$ .....	37
Figure 4.4: Inline force time series with and without the slamming effect. (Ghadirian & Bredmose, 2019) .....	38
Figure 4.5 Dimensionless pressure impulse at every discretized point for the realistic sea state .....	39
Figure 4.6 Time series for the drag and inertia force. ....	40
Figure 4.7 Time series of the combined drag and inertia force (Morrison force).....	41
Figure 4.8 Total force time history with DNVGL impact force .....	42
Figure 4.9 Total force time history with IEC impact force .....	42

Figure 4.10 Comparison of slam coefficient time histories. ....	43
Figure 4.11 Time history of the normalized DNVGL impact force.....	44
Figure 4.12 Time history of the normalized IEC impact force. ....	45

# 1 Introduction

## 1.1 Background

In 2021 the European Commission promoted several ambitious regulations to transform the energy supply and reduce greenhouse gas emission with at least 55% within 2030, and climate neutrality in 2050. The reason is to convert Europe to a low-emission society and to become the first climate-neutral continent. The contribution from renewable energy sources like solar, wind and hydro energy has increased in several countries the last few years, where offshore wind energy has become one of the fastest growing renewable energy sources (European Commission, 2020).

In 2020 wind energy production was 458 TWh, but wind resources in Europe have the potential to extract 25,000 TWh solely from offshore wind power. The average size and power of offshore wind turbines has increased significantly since 2000, when the average capacity was around 2 MW and in 2020 the average capacity was more than 8 MW. There is a larger potential in offshore wind than in onshore wind, due to higher normal wind speeds and steadier wind environment. The wind turbine size can be increased offshore without the same repercussion that would have been the case onshore, with possible objections from municipalities and residents. The North Sea is the most active region for installing wind turbines and will continue to be so with 80 % of all planned installations over the next five years located in the North Sea (WindEurope & ETIPWind, 2021).

Share of substructure types for wind turbines installed\*

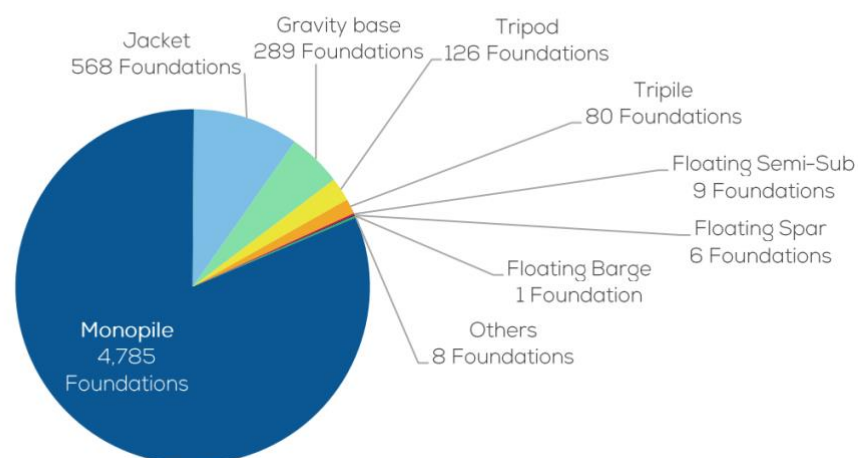


Figure 1.1 Share of substructure types (WindEurope & ETIPWind, 2021)

Monopiles are the preferred foundation for offshore wind turbines where 81.2% of all foundations installed in Europe were monopiles at a water depth of around 20-40 m (WindEurope & ETIPWind, 2021). Monopiles are the most common foundation due to its low cost, minimal footprint on the seabed and low design requirement. Unlike other types of foundations (Jackets, tripods), they do not require advanced techniques or preparation of the seabed prior to their installation. Also, the relatively simple shape of a monopile can keep its construction cost down, though it requires a large tube diameter. The monopile is usually driven into the seabed using a hydraulic hammer, then the transition piece is installed using a bolted or grouted connection on top of the monopile. The limitations regarding monopiles are related to higher water depths. When the water depth increases the required stiffness of the monopile also increases, which results in the use of piles with larger diameter. The installation of these piles can be difficult due to pile driving capacity, material size and availability.

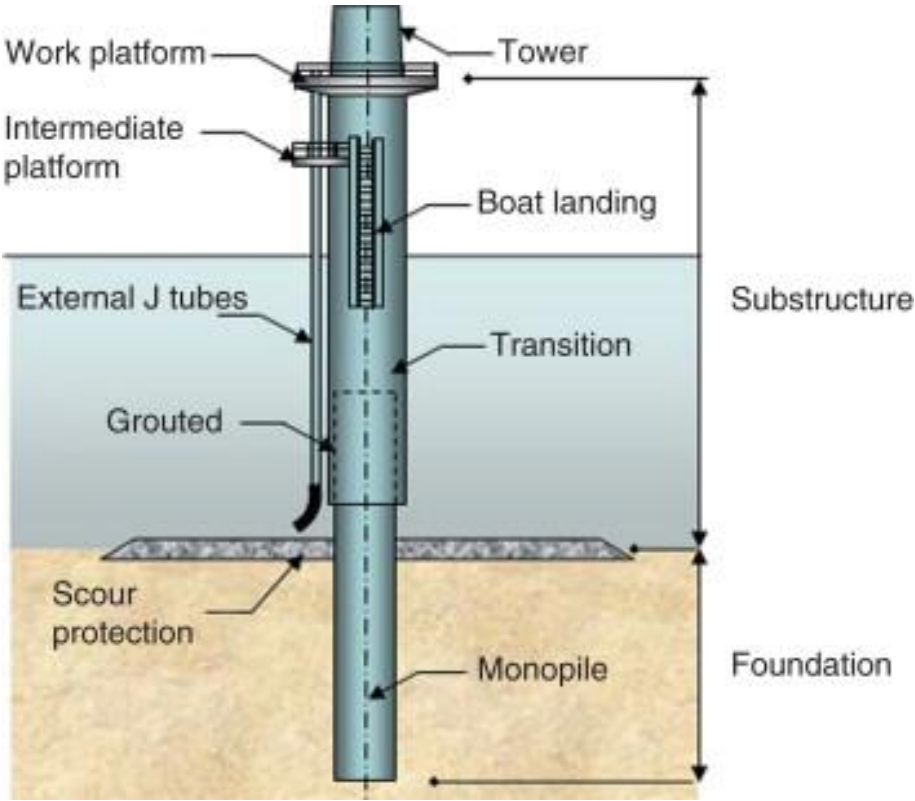


Figure 1.2 Monopile structural foundation (Leite, 2015)

Offshore structures are subjected to different loads such as wind, waves and current, and in the design of these structures it is essential that these environmental loads are taken into account. The wave loads are the loads that causes the most severe damage to these structures, and there are several model tests that indicates that breaking wave loads generate higher impact loads



than what are suggested in some guidelines and standards. In the case of breaking waves, the horizontal water particles moves faster than the phase velocity of the wave. This phenomenon occurs when the water on the top moves faster than the wave itself and ends up breaking. This behavior of the wave creates more irregular and forward-moving waves that can impact a structure. This can cause severe damage to a structure if not considered properly in the design.

Since these offshore wind turbines are installed at shallow to intermediate water depth, they are subjected to rough sea states, breaking waves, wave run-up and scour. The high impact forces that are generated by breaking waves on the substructure of an offshore wind turbine can affect the turbine's performance and fatigue life. This will affect the offshore wind turbine structure design, which could increase the stiffness of the structure and the cost. The possibility of extreme wave loads acting on the structure, requires correct estimations of Ultimate Load States (ULS) to prevent over estimated safety factors.

There are different approaches to calculating the extreme wave loads acting on circular cylinders. The pressure impulse model investigated by Ghadirian & Bredmose (2019), is the time integral of the pressure during a short time scale impact on circular cylinders. The model has relative impact height, cylinder radius and crest length as variables, where the maximum angle of impact is a parameter that can be changed to achieve the right force impulse. In current standards for offshore wind turbines, such as IEC 61400-3 (2009), DNVGL-RP-C205 (2017), DNVGL-ST-0437 (2016) and DNV-OS-J101 (2014), the guidelines recommend the Morison equation for calculating ULS on frame structures. The wave loads are determined with the drag and inertia force as the two components contributing to the total force. For the case with breaking wave loads, a third component is added to the Morison equation, the slamming force, which is a high impulse short duration force generated by the breaking wave hitting the structure. For calculating the impact load from breaking waves IEC 61400-3 (2009) recommends Wienke and Oumeraci's model (2005), and the DNVGL standards recommend Weynberg & Campbell's model (1980).

## **1.2 Objectives**

The objective of this report is to determine and investigate the breaking wave loads using DNVGL and IEC standards and the pressure impulse model, with the intention of comparing the results and determine any overprediction of force impulse.

To achieve the main objective of this thesis, several sub-objectives will be performed:

- Investigate standards and previous work that has been done on the field to ensure that the correct method is implemented by doing a background study.
- Define parameters such as sea state, structure dimensions, water depth and force coefficients to best compare the results with the pressure impulse model.
- Calculate the pressure impulse by applying the pressure impulse model with a MATLAB script provided by Assoc. Prof. Charlotte Obhrai.
- Calculate the inertia and drag force acting on column elements of the structure and sum up over the total length of the submerged structure to get the total force.
- Calculate the slamming force from the breaking wave, and the impact duration of the slamming force.
- Discuss and compare the results obtained.
- Conclude and suggest further work that can be done to compare these different methods more extensively for calculating wave loads on structures.

### **1.3 Structure of this paper**

This thesis is presented in 6 chapters. Chapter 1 contains general description of offshore wind turbines, the monopile structure and wave loads associated with breaking waves and calculation models. In chapter 2, background theory on previous numerical and experimental studies conducted related to breaking waves and wave forces, including a general description of Ghadirian & Bredmose (2019) pressure impulse model. In chapter 3, the mathematical formulation for the Morison equation is introduced, as well as Wienke and Oumeraci`s (2005) and Campbell & Weynberg`s (1980) calculation method for the slamming force. The mathematical formulation for the pressure impulse model is also included. Chapter 4 contains the reproduced results of the pressure impulse from Ghadirian & Bredmose (2019). The drag, inertia, and the slamming force according to IEC and DNVGL is also presented in chapter 4. Chapter 5 and 6 contains discussion, future work, and conclusion.

## 2 Background

### 2.1 Theoretical Models

There are different wave impact models that can be used to predict the slamming load on offshore structures. Von Karman's method is one of the most common theoretical models to investigate the impact force on slender cylinders (von Karman, 1929). The von Karman method is stating that the cylinder is approximated by a flat plate, where the width of the flat plate is equal to the immersed width of the cylinder. The impact force is calculated by integrating the force over the impact area height. The effect that von Karman didn't consider was the pile-up effect, which Wagner (1932) explained as the water surface "pile-up" along the pile surface of the structure. Wagner's model includes the pile-up effect, which increases the slamming coefficient and thereby the impact force. Later Goda et al. (1966) implemented the von Karman method to calculate impact forces acting on the vertical cylinder and predicted the time history of the impact force using this method. The von Karman method is also implemented by Tanimoto et al. (1987) with the assumption that the force distribution has a triangular shape along the pile. Wienke & Oumeraci (2005) presented a theoretical model where the wave load is divided into a dynamic and a quasi-static component and the peak pressure is based on the Wagner theory.

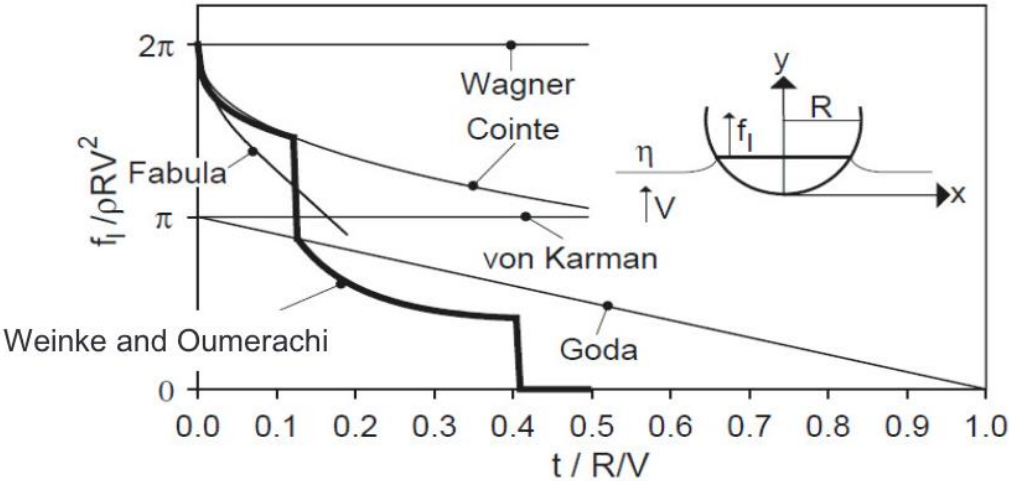


Figure 2.1 In-line force comparison (Wienke & Oumeraci, 2005)

Cointe & Armand (1987) considered a parabolic shape of the body to predict the immersed width of the cylinder, where the decrease of the impact force with time is slower than the one Fabula (1957) predicted, which is approximated by the body of an elliptical shape.

## 2.2 Numerical Simulations

Christensen, Bredmose and Hansen (2005) numerically analyzed the wave forces and wave run-up on offshore wind turbine foundations with the use of Navier Stokes solver. They compared the results from the Navier Stokes solver with the wave force and wave run-up estimated by Kriebel (1992) and Kriebel (1998), and the comparison showed good agreement.

Bredmose & Jacobsen (2010) used the numerical model called OpenFOAM to investigate the wave impact from well-developed breaking waves to less developed breaking waves on offshore wind turbines. The in-line force obtained from the computational fluid dynamic (CFD) model was then compared to estimations determined from the Morison equation, with varying focus points for the wave group.

Wu et al. (1994) used the Volume of Fluid (VOF) concept to numerically simulate the impact load on a vertical wall without entrapped air pocket. There were also numerical simulations implementing entrapped air without qualitatively reliable results, due to the models lack of ability to account for the incompressible flow. Mokrani et al. (2010) used a combination of Navier stokes equation and VOF concept called NS-VOF to numerically simulate impact force from plunging waves breaking in front of a vertical wall. Corte and Grilli (2006) modeled the pressure impact from extreme waves acting on a circular structure with the use of Finite Volume – Volume of Fluid approach (FV-VOF) for two-phase flow (water and air). Nielsen et al. (2008) numerically tested three-dimensional (3D) wave run-up with the fully non-linear NS-VOF model and compared the results with a physical test model with the same conditions. Bredmose & Jacobsen (2011) computed the breaking wave impact and the run-up flow on a vertical structure using the VOF method. They also computed the impact from vertical run-up on a monopile for different platform levels.

Hildebrandt and Sriram (2014) investigated the effects of the vortex and pressure impulse on a cylinder by using a numerical model that is based on the weak coupling of Fully Nonlinear potential flow theory (FNPT), ANSYS-CFX and Finite Element Method (FEM). The pressure impulse was estimated on the outside of the cylinder for various heights and compared to the experimental results with good agreement. Investigations were conducted by Chen et al. (2014) on the performance of OpenFOAM when applied to non-linear waves interacting with offshore structures. Based on comparisons with Danish Hydraulic Institute`s (DHI) physical

experiments, the OpenFOAM showed good capabilities of solving the non-linear waves interacting with offshore structures.

Devolder et al (2017) applied OpenFOAM to investigate a monopile inside a numerical wave flume subjected to wave run-up in regular waves. In order to best simulate the flow around the monopile, they also applied the buoyancy modified disturbance model,  $k\omega$ -SST, which prevented the wave height to decrease excessively over the wave flumes length. The results of the wave run-up showed agreement with the analytical formulations and the experimental data. Veic and Sulisz (2018) analyzed the pressure distribution for two breaking wave cases with the use of a combined numerical model of potential flow and Navier-Stokes/VOF solution. The difference for the two generated waves were the steepness of the wave front. The pressure increases significantly under the overturning wave jet, which results in peak impact pressure in this region with a slamming coefficient of  $C_s=2\pi$ . The peak impact pressure is detected to be four times higher than at the beginning of impact.

### **2.3 Experimental Models**

The study conducted by Goda et al. (1966) focused on the impact forces on triangular and circular vertical cylinders. They presumed that the change in the water mass momentum caused by a vertical wave front led to the increase in the impact force. However, they did not take into account the impact force rising time. The experiments conducted by Sawaragi & Nochino (1984) discovered that the impact force of a breaking wave can rise as the wave front changes its shape. It also affects the magnitude of the impact force depending on the breaking pattern and breaking point of the wave. They found that the vertical distribution's peak values are triangular shaped which appears at the height of around 70% of the wave crest (Chella et al. 2012). They then calculated the total force by taking into account the impact force, Morison force, and static pressure. The difference in water level at the cylinder between seaward and leeward caused the static pressure. It was noted that the biggest value of the force is seven times greater than that of the Morisons force. For the estimation of both the inertia and drag coefficient, the difference in phase between inertia force and the water particle acceleration needs to be considered.

Previous tests that have been performed on small scale cylinders with diameters ranging from 5-10 cm. Wienke & Oumeraci (2005) carried out tests on larger scale cylinders in a wave flume with a water depth varying between 4 m and 4.25 m. The generated wave height was up to 2.8 m, impacting a steel cylinder with a diameter of 0.7 m installed on the bottom of the flume. They discovered that the effect from pile-up affects the magnitude and duration of the impact force. It was also noted that the distance from the cylinder to the breaking wave influences the magnitude of the impact force. The impact force is also proportional to the curling factor which is affected by the breaker front inclination angle and the cylinders inclination angle.

## **2.4 Pressure Impulse Model**

The design process for offshore structures involves the calculation of the slamming force of wave impacts. Engineering models are commonly used for this process. These models take into account the various factors that affect the peak pressure of the impact, such as Wienke & Oumeraci (2005) and Campbell & Weinberg (1980). The force impulse model developed by Wienke & Oumeraci is overpredicted by around 190%. This is mainly due to the time span and maximum force magnitude that are predicted. The time integrated force impulse can be used to predict the response of an object after it has been impacted. Usually, the impact's duration is very short.

Based on the existing model of Cooker & Peregrine (1995), Ghadirian & Bredmose (2019) developed a pressure impulse model for waves impacting vertical surfaces and cylinders. The model takes into account the primary reaction due to the force impulse theory, instead of the peak force value. Depending on the characteristics of the impact, the peak pressure of an impulse can vary significantly. This variability can be caused by the momentum conservation. The time integral of the pressure, on the other hand, can show a smaller variability. The time-integrated force impulse can be used to predict the response of a structure after it has been hit for a short duration. The pressure impulse theory can also be used in this situation to derive the spatial distribution of the force over the structure. The model is derived from a simple geometry and has several effective parameters, such as the cylinder radius, impact height, and crest length. The maximum angle of impact, which is free, is the parameter that can be used to produce the right force impulse.

## **2.5 DNVGL and IEC Standards**

### **2.5.1 IEC 61400-3**

There are different guidelines to calculating the breaking wave load on vertical cylindrical structures. IEC 61400-3 (2009) guidance to calculate hydrodynamic loads states that the hydrodynamic loads can be classified as viscous drag load, inertia loading and slap and slam loading. The viscous drag load is associated with the vortices created in the flow passing the structure, where the viscous drag force is proportional to the square of the incoming fluid velocity. The inertia loading acting on the structure is caused by interaction between the structure and the accelerating incoming fluid, also the pressure gradient in the fluid affects the inertia loading. Slap and slam loading is defined as two different components where the slam load occurs when a wave passes a horizontal structure, and the structure is engulfed by the passing wave. The slap loading component is associated with the loads created by breaking waves acting perpendicular to the wave direction.

IEC 61400-3 (2009) states that the Morison (1953) equation is the preferred calculation method for estimating the inertia load and viscous drag load acting on a vertical structure. The condition for this statement is that the structure must be small compared to the wavelength and therefore the water particle motions can be seen as only locally affected by the structure. The force acting on the vertical structure can then be determined from the drag and inertia terms for non-breaking waves. When calculating the breaking wave force the IEC standard adds a third term called the slap and slam load. The calculation of the slamming load, also called impact load suggested in IEC 61400-3 (2009) is Wienke & Oumeraci's model (2005) based on Wagner (1932) theory. This model improves the approximation of the wetted surface of the cylinder by applying a polynomial stepwise function for circular shaped cylinders. When the impact is at an angle the model suggest that the shape of the body needs to be considered as an elliptical shape instead of a circular shape.

### **2.5.2 DNVGL-RP-C205, DNVGL-ST-0437 and DNV-OS-J101**

There are different DNVGL standards which mentions and explain the non-breaking and breaking wave forces acting on a monopile. DNVGL-RP-C205 (2017) presents recommended practices and guidelines for environmental conditions and environmental loads, where this standard gives an insight into both breaking wave loads, and non-breaking wave loads for different structures at sea. DNVGL-ST-0437 (2016) contain principles, requirements and guidance for load and site conditions for wind turbines, where this standard gives guidance on non-breaking wave loads and refers to the DNVGL-RP-C205 (2017) for the guidance on calculating breaking wave loads in section 4, calculation of loads. DNV-OS-J101 (2014) provides principles and guidance on the design of offshore wind turbine structures, where the wave loads generated both from breaking and non-breaking waves are thorough explained in chapter 4, loads and load effects.

The DNVGL-RP-C205 (2017), DNVGL-ST-0437 (2016) and DNV-OS-J101 (2014) standards all states that the Morison equation is the formula that is preferred for calculating inertia and drag loads in waves acting on a cylinder structure, with the requirement that the dimension of the structure is small compared to the wavelength. The condition set for this requirement is  $D < 0,2\lambda$ , where  $\lambda$  is the wavelength and D is diameter of the monopile. These standards states that the inertia force is proportional to the horizontal water particle acceleration, and the drag force is proportional to the square of the horizontal water particle velocity. DNVGL-RP-C205 (2017) and DNVGL-ST-0437 (2016) describes the procedure to calculate the shock pressure from breaking wave impact acting on a vertical surface. The impacting force is proportional to the square of the impact velocity, which is 1.2 times the phase velocity of the highest breaking wave. The duration of the impact force from breaking waves are defined as short duration high impact where the wave is a plunging wave breaking in front of the monopile.



### 3 Mathematical Formulation

#### 3.1 Definition of Breaking Waves

When a wave gains more energy the breaking of the wave is initiated, the wave then becomes unstable. The wave systems energy is focused on the crest of the wave during the breaking process of the wave. Waves breaking on site may occur depending on steepness, wave height, seabed slope, wave period and water depth. Breaking of waves can be classified in different forms such as plunging, surging, spilling, and collapsing, where collapsing is a combination of surging and plunging. According to DNVGL-ST-0437 (2016) the occurring types of breaking waves can be defined mathematically as follows:

$$\beta = \frac{H_b}{gT^2m} \quad (3.1)$$

Where:

$H_b$  – Wave height at breaking

$m$  – Beach slope

$T$  – Wave period

$g$  – Gravitational acceleration

- Spilling breakers are characterized by foam spilling from the crest down on the forward face of the wave. These types of breaking waves occur on beach slopes or in deep water. Usually spilling breakers form when  $\beta > 5$ .
- Plunging breakers are characterized by a well-defined jet of water forming from the crest and falling onto the water surface ahead of the crest. The plunging breakers occur on moderately steep beach slopes, when  $0,1 < \beta < 5$ .
- Surging breakers are characterized by foam forming near the beach surface, where these types of breakers occur on relatively steep beaches. The surging breakers form when  $\beta < 0,1$ .
- The collapsing breakers are characterized by the wave foams lower down the forward face of the wave. These collapsing breakers are formed when  $\beta \sim 0,1$ .

Plunging and spilling breakers have a tendency of creating higher impulse loads and higher pressure, which gives these types of breakers a greater importance than the other conditions.

### 3.2 Inertia and Drag Force

Morrison Equation is often used to calculate the non-breaking wave force on slender piles, where the equation is the sum of inertia and drag force. According to Wienke & Oumeraci (2005), the inertia force depends on the acceleration of the water particles and the drag force depends on the square of the water particle velocity. The coefficient of inertia  $C_M$  and coefficient of drag  $C_D$  are empirically determined from Roughness number, Keulegan-Carpenter number and Reynolds number.

The Morrison equation is given as follows:

$$F_{Total} = F_D + F_I \quad (3.2)$$

$$F_D = \int_{-d}^0 \frac{1}{2} \rho C_D D u(z, t) |u(z, t)| dz \quad (3.3)$$

$$F_I = \int_{-d}^0 \rho C_M \frac{\pi D^2}{4} \dot{u}(z, t) dz \quad (3.4)$$

Where:

$F_D$  – Drag force

$F_I$  – Inertia force

$C_D$  – Drag coefficient

$C_M$  – Inertia coefficient

$\rho$  – Mass density of water

D – Pile diameter

$u$  – Water particle velocity

$\dot{u}$  – Water particle acceleration

When comparing the results from the pressure impulse model to realistic wave impact Ghadirian & Bredmose (2019) used a sea state of  $H_s = 9.5 \text{ m}$  and  $T_p = 12 \text{ s}$ , with a water depth of 33 m and a cylinder diameter of 7 m. Calculating the total force from the Morison equation, there are some parameters that need to be defined. When calculating the wavelength, the given parameters of the sea state was not sufficient. In finite water depth the wavelength,  $\lambda$ , is determined by the transcendental equation mentioned in DNV-OS-J101 (2014). The wavelength was calculated by using the solver function in Excel. The wave number,  $k$ , is defined as number of radians per unit distance where the distance is the wavelength and the frequency equal to  $2\pi$ . The value,  $z$ , is the depth below still water level (SWL) measured negatively downwards. Angular wave frequency,  $\omega$ , is the angular displacement of the wave per unit time, where the time is the wave period.

$$\lambda = \frac{gT^2}{2\pi} \tanh\left(\frac{2\pi d}{\lambda}\right) \quad (3.5)$$

$$k = \frac{2\pi}{\lambda} \quad (3.6)$$

$$\omega = \frac{2\pi}{T} \quad (3.7)$$

$$\theta = kx - \omega t \quad (3.8)$$

Where:

$\lambda$  – Wavelength

$k$  – Wave number

$T$  – Wave period

$d$  – Water depth

$\omega$  – Angular wave frequency

$g$  – Gravitational acceleration

To utilize the Morison equation, the horizontal water particle velocity and acceleration must be defined. In DNVGL-RP-C205 (2017) these values are computed using the Airy wave theory:

$$u = \frac{\pi H \cosh[k(z + d)]}{T \sinh(kd)} \cos \theta \quad (3.9)$$

$$\dot{u} = \frac{2\pi^2 H \cosh[k(z + d)]}{T^2 \sinh(kd)} \sin \theta \quad (3.10)$$

Where:

H – Significant wave height

z – Depth below SWL

When a vertical cylinder is exposed to drag and inertia force due to waves, the horizontal velocity and acceleration will change both in z-direction (vertically) and in time. When evaluating the force, with the use of Morison's equation, of a small section of the cylinder at each depth and then summarized over the length of the submerged cylinder to get the total force.

$$dF_D(z, t) = \sum_{z=-d}^{z=0} \frac{1}{2} \rho C_D D u(z, t) |u(z, t)| dz \quad (3.11)$$

$$dF_I(z, t) = \sum_{z=-d}^{z=0} \rho C_M \frac{\pi D^2}{4} \dot{u}(z, t) dz \quad (3.12)$$

One of the problems with using the Morison's equation is the uncertainty and scatter in values of the drag and inertia coefficients. There is a degree of correlation between the Reynolds number, the Keulegan-Carpenter number and the coefficients, but the scatter and uncertainty still remain. There have been many experiments to measure the drag and inertia coefficient values for different flows, but these results must be used with caution when applied in wave force prediction. The most useful estimations have been related to full-scale model experiments at ocean sites. Ghadirian & Bredmose (2019) used a drag coefficient of  $C_D = 1.0$ , and inertia coefficient of  $C_M = 1.79$  by applying recommended practices for smooth steel cylinders.

### 3.2.1 Definition of Drag and Inertia Coefficient

The drag coefficient is determined from the function of the Reynolds number,  $Re$ , and the cylinder surface roughness,  $k$ . Increased  $k$  value results in increase of the drag coefficient and resulting in increased drag force. The Reynolds number is dimensionless and is given by the following formula:

$$Re = \frac{uD}{\nu} \quad (3.13)$$

Here,  $D$  is the cylinders diameter,  $\nu$  is the kinematic viscosity of the water and  $u$  is the velocity of the horizontal water particle. Since the velocity changes with depth, the drag coefficient also changes with depth. This is normally not practices, instead one drag coefficient is determined for the whole length of the structure. Figure 3.1 shows that the drag coefficient,  $C_d$ , changes with different roughness,  $k$ , and Reynolds number,  $Re$ .

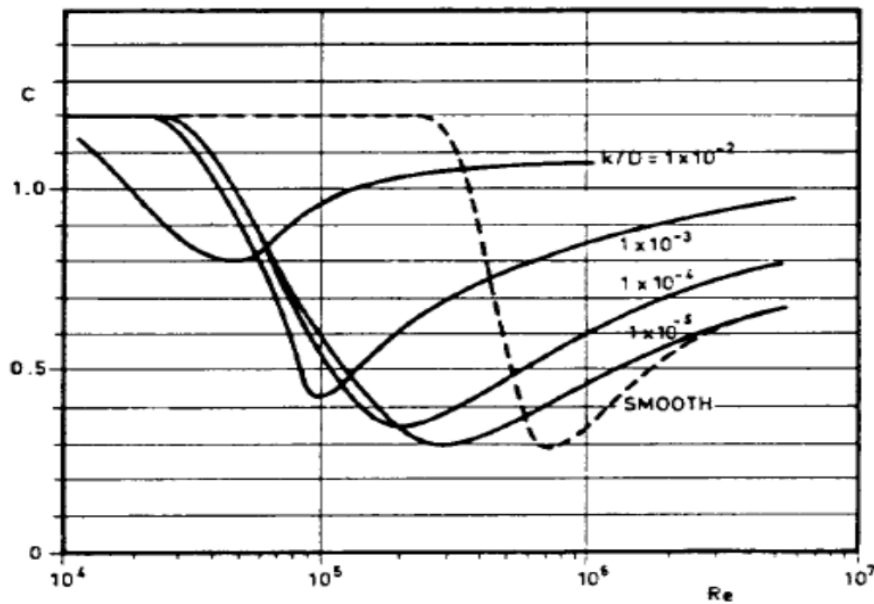


Figure 3.1 Drag coefficient for fixed circular cylinder for steady flow in critical flow regime, for various roughnesses (DNVGL-RP-C205, 2017)

The Keulegan-Carpenter number is a parameter that can be used to determine the magnitude of the wave forces, and is calculated by the following formula at still water level:

$$KC = \frac{\pi H}{D} \quad (3.14)$$

Where D is the cylinder diameter and H is the wave height. When the KC number is low, which is typical for large diameter cylinders or a slow flow past the cylinder, the mass term is dominant. For large KC numbers the flow past the structure is rapid or small diameter cylinder, and the drag term will be dominant.

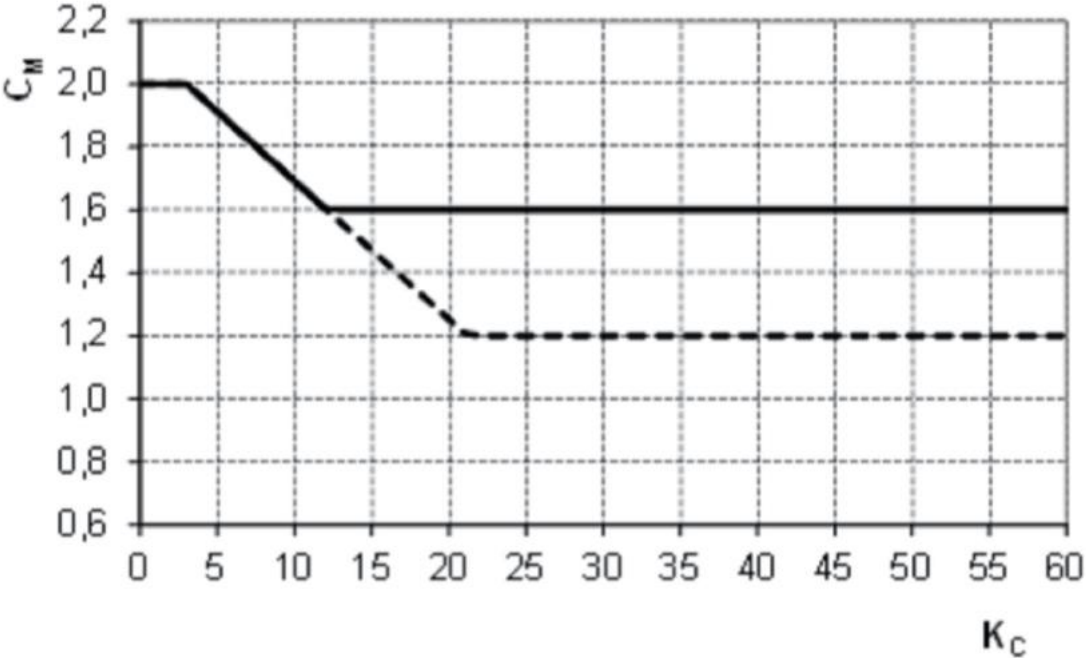


Figure 3.2 Mass coefficient as function of KC number for smooth (Solid line) and rough (Dotted line) cylinder (DNVGL-RP-C205, 2017)

The inertia coefficient is related to the KC number and the roughness, k, of the cylinder surface. The inertia coefficient is independent for KC values below 3,  $KC < 3$ , and the inertia coefficient can be taken as,  $C_M = 2,0$  for both rough and smooth cylinders. For KC values above 3,  $KC > 3$ , the inertia coefficient is determined from the following formula:

$$C_M = \max \left\{ \begin{matrix} 2 - 0.044(KC - 3) \\ 1.6 - (C_{DS} - 0,65) \end{matrix} \right. \quad (3.15)$$

Where  $C_{DS}$  is the value of roughness with  $C_{DS} = 0,65$  for smooth cylinders and  $C_{DS} = 1,05$  is the value for rough cylinders. Intermediate roughness is decided with linear interpolation between the curves for smooth and rough surface cylinders.

For large KC-numbers, the dominant force is the drag compared to inertia, and the inertia coefficient,  $C_M$ , for large KC numbers are:

$$C_M = \begin{cases} 1.6 & \text{for smooth cylinders} \\ 1.2 & \text{for rough cylinders} \end{cases} \quad (3.16)$$

### 3.3 Slamming Force

When calculating the total wave force on a vertical cylinder caused by a breaking wave, a common engineering practice is to add the slamming force to the Morrison equation. The slamming force is an impact force which implies that the wave breaks against the structure. The slamming force is added to the Morrison equation, and is expressed in the most general case as follows:

$$F_{Total} = F_D + F_I + F_S \quad (3.17)$$

$$F_S = \lambda \eta_b \rho_w R C_b^2 C_S \quad (3.18)$$

Where:

$F_S$  – Slamming force

$C_S$  – Slamming force factor

$C_b$  – Breaking wave celerity

$\lambda$  – Curling factor

$\eta_b$  – Max free surface elevation

$R$  – Radius of the cylinder

$\rho_w$  – Density of water

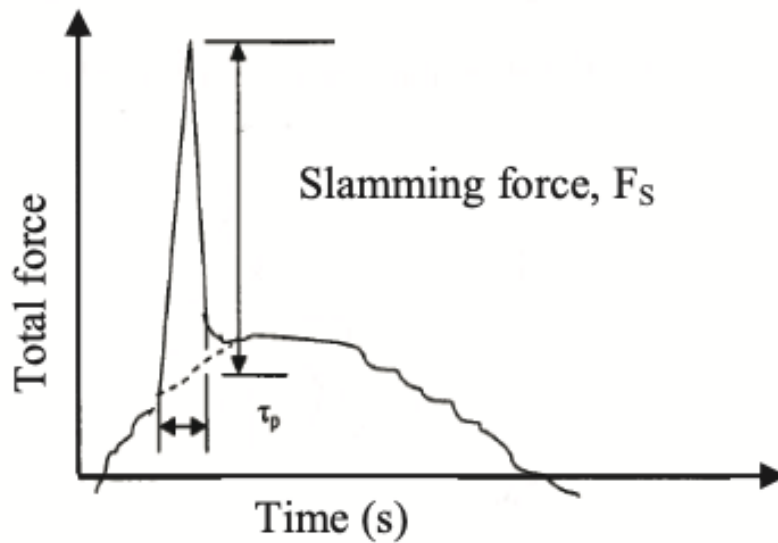


Figure 3.3: Nature of the slamming force (Chella et al., 2012)

### 3.3.1 Wagner and von Karman`s Theory

For circular and hollow cylinders, the water is acting like an even surface hitting an even plate. Von Karman was one of the first to investigate the impact force on a cylinder, where a flat plate with the width of the immersed width of the cylinder and integrating the force over the height of the impact area results the impact force (Chella et al., 2016).

Von Karman`s formulation of mass flow against a flat plate account for the added hydrodynamic mass. Wagner`s formulation also considers the pile-up effect which is a result of the flow on the sides of the flat plate, also described as misshaping of the water free surface. The pile-up effect will decrease the time interval of the impact and increase the slamming force.

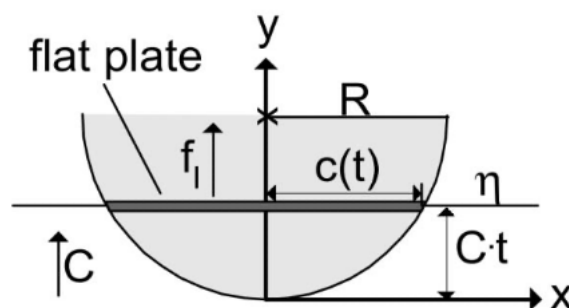


Figure 3.4: Von Karman`s formulation (Wienke & Oumeraci 2005)



The slamming coefficient  $C_S$ , also referred to as maximum line force is according to Von Karman  $C_S = \pi$ , and according to Wagner the slamming coefficient is,  $C_S = 2\pi$ .

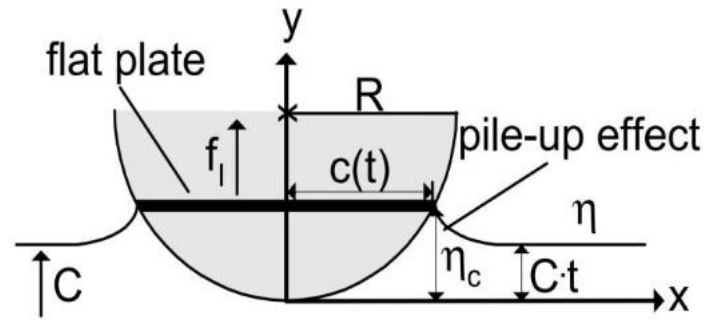


Figure 3.5: Wagner's formulation (Wienke & Oumeraci, 2005)

### 3.3.2 IEC Standard - Wienke and Oumeraci's Model

Wienke & Oumeraci (2005) is the preferred theoretical model used in IEC 61400-3 (2009) and implements the Wagner theory for the theoretical calculation of the peak pressure. Applying a potential flow model and neglecting the force created by gravity as well as the surface tension, Wienke & Oumeraci (2005) created a new analytical model to determine the impulse force. The impact force on piles is usually estimated using Goda et al. (1966) approach:

$$F_S = \lambda \eta_b \rho_w R C_b^2 C_S$$

$$C_S = 2\pi \left(1 - \frac{C_b}{R} t\right) \quad (3.19)$$

The height of the impact area is expressed as  $\lambda * \eta_b$ , where  $\eta_b$  is the wave elevation at the breaking point, and  $\lambda$  is the curling factor that express the magnitude of the wave crest active in the slamming load. The distribution of the slamming force is equally along the height of the impact area so that the expression of the impact becomes:

$$F_S = \rho_w R C_b^2 2\pi \left(1 - \frac{C_b}{R} t\right) \quad (3.20)$$

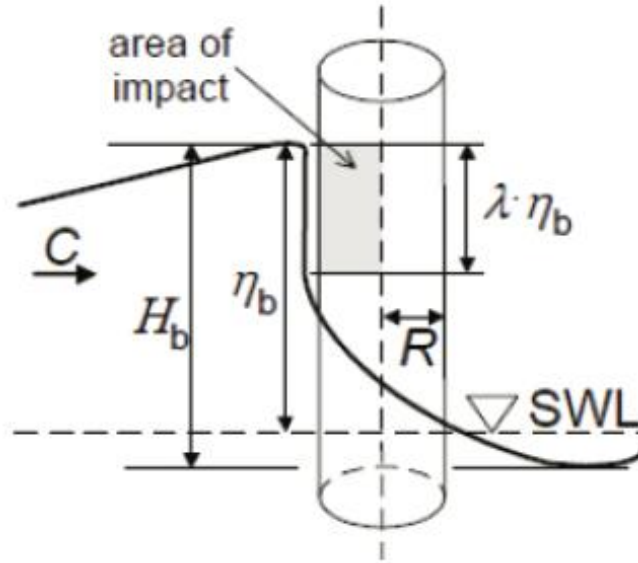


Figure 3.6: Impact force on circular cylinder (Wienke & Oumeraci, 2005)

The maximum slamming force is expressed in the starting phase of the impact from the wave, so  $t$  is set equal to zero which corresponds to the presumptions made by von Karman,  $t=0$  and the expression becomes:

$$F_S = \rho_w R C_b^2 2\pi \quad (3.21)$$

When calculating the impact force during the total duration of the impact both IEC 61400-3 (2009) and Wienke & Oumeraci (2005) states that the force normal to the cylinder axis is expressed as:

$$F_S = \lambda \eta_b \rho_w R C_b^2 \left( 2\pi - 2 \sqrt{\frac{C_b}{R}} t \left( \tanh^{-1} \sqrt{1 - \frac{C_b}{2D} t} \right) \right) \quad (3.22)$$

For  $0 \leq t \leq \frac{R}{8C_b}$

$$F_S = \lambda \eta_b \rho_w R C_b^2 \left( \pi \sqrt{\frac{R}{6C_b t_s}} - \sqrt{\frac{8C_b}{3R}} t_s \tanh^{-1} \sqrt{1 - \frac{C_b}{R} t_s \sqrt{\frac{6C_b}{R} t_s}} \right) \quad (3.23)$$

For  $\frac{R}{8C_b} \leq t_s \leq \frac{13R}{32C_b}$ , where  $t_s = t - \frac{R}{32C_b}$

Where the total impact duration, also called total slam duration is expressed as:

$$T = \frac{13 R}{32 C_b} \quad (3.24)$$

### 3.3.3 DNVGL Standard - Campbell and Weynberg`s Model

The maximum slamming force on a vertical circular cylinder can be predicted according to DNVGL-RP-C205 (2017) by applying Campbell & Weynberg`s (1980) model:

$$F_s = \frac{1}{2} \rho_w A_{exposed} C_b^2 \left( 5.15 \left[ \frac{D}{D + 19 C_b t} + \frac{0.107 C_b t}{D} \right] \right) \quad (3.25)$$

For undisturbed waves the phase velocity is expressed as:

$$C = \sqrt{\frac{g}{k} * \tanh(kd)} \quad (3.26)$$

Impact velocity for undisturbed waves is expressed as phase velocity of the most probable highest wave times 1,2 as shown below:

$$C_b = 1,2 * C \quad (3.27)$$

Total duration of the impact for a plunging wave breaking in front of the structure may be taken as:

$$T = \frac{D}{C_b} \quad (3.28)$$

The area exposed to impact pressure can be taken as 0,25 times the most probable highest breaking wave, and a width with a sector of 45 degrees as shown in figure 3.5. The most probable largest breaking wave height can be expressed as 1,4 times the most probable largest significant wave height.

$$A_{exposed} = \frac{D\pi H_b}{8 \cdot 4} \tag{3.29}$$

$$H_b = 1,4 * H_s \tag{3.30}$$

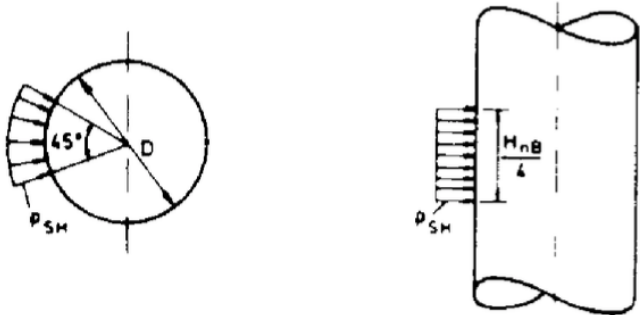


Figure 3.7 Area exposed to shock pressure (DNVGL-RP-C205, 2017)

### 3.4 Pressure Impulse Method

To calculate the pressure impulse for a slamming wave on a vertical wall the following equation is used:

$$\frac{P}{\rho U H} \left( \frac{x}{H}, \frac{y}{W}, \frac{z}{H} \right) = f \left( \frac{b}{H}, \mu, \frac{W}{H} \right) \quad (3.31)$$

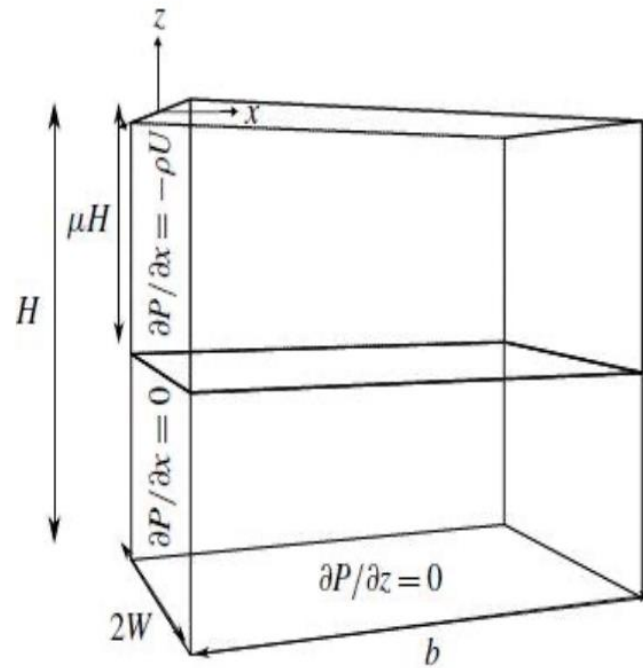


Figure 3.8 Definition sketch for 3D block impact on a vertical wall.  
(Ghadirian & Bredmose, 2019)

Where:

$\frac{b}{H}$  – Relative length of the block

$\mu$  – Relative height of the impacting zone

$\frac{W}{H}$  – Relative width of the block

The vertical wall is the simplest shape of a structure to analyze the impacting pressure impulse, where the water is in contact with the wall at  $-H \leq z \leq -\mu H$  and the wave hits the wall in the  $-\mu H \leq z \leq 0$  region. The location of the vertical wall is at  $x = 0$ . The region of the width is expressed as  $0 \leq x \leq b$ , and the region of the depth is expressed as  $-W \leq y \leq W$ .

Using Fourier series and separation of variables the Laplace equation is solved, and can be written as:

$$P(x, y, z) = \sum_{m=1}^{\infty} \sum_{n=1}^{\infty} \left( A_{mn} \cos\left(\frac{L_m y}{W}\right) \sin\left(k_n \frac{z}{H}\right) \frac{\sinh\left(\sqrt{L_m^2 \left(\frac{H}{W}\right)^2 + k_n^2} \left(\frac{b-x}{H}\right)\right)}{\cosh\left(\sqrt{L_m^2 \left(\frac{H}{W}\right)^2 + k_n^2} \frac{b}{H}\right)} \right) \quad (3.32)$$

Where  $L_m = (m - 1/2)\pi$ ,  $k_n = (n - 1/2)\pi$  and

$$A_{mn} = 4\rho UH \frac{(\cos(k_n \mu) - 1) \sin(L_m)}{k_n L_m \sqrt{L_m^2 \left(\frac{H}{W}\right)^2 + k_n^2}} \quad (3.33)$$

To calculate the pressure impulse from axisymmetric impact for a slamming wave on a vertical cylinder the following equation is used:

$$\frac{P}{\rho UH} \left(\frac{r}{H}, \frac{z}{H}\right) = f\left(\frac{b}{H}, \mu, \frac{a}{b}\right) \quad (3.34)$$

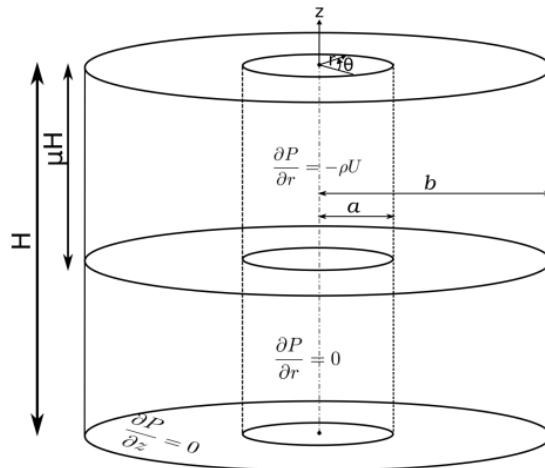


Figure 3.9 Definition sketch for axisymmetric impact on a vertical cylinder. (Ghadirian & Bredmose, 2019)

Where:

$\frac{b}{H}$  – Relative length of the impacting wave

$\mu$  – Relative height of the impacting zone

$\frac{a}{b}$  – Relative inner radius

The water height on the cylinder structure is the same as for the vertical wall, where the water is in contact with the cylinder at  $-H \leq z \leq -\mu H$  and the wave hits the cylinder in the  $-\mu H \leq z \leq 0$  region. The outer radius of the fluid impacting the cylinder is expressed as b, and the radius of the actual cylinder is expressed as a.

The cylindrical coordinate system is used to solve the Laplace equation as follows:

$$P = \sum_{n=1}^{\infty} \left( A_n \frac{I_0\left(k_n \frac{r}{H}\right) + \alpha_n K_0\left(k_n \frac{r}{H}\right)}{\partial_r \left( I_0\left(k_n \frac{r}{H}\right) + \alpha_n K_0\left(k_n \frac{r}{H}\right) \right)_{r=a}} \sin\left(k_n \frac{z}{H}\right) \right) \quad (3.35)$$

Where  $k_n = (n - 1/2)\pi$ , the partial derivative is expressed as  $\partial_r$  with respect to r,  $I_0$  and  $K_0$  are the first and second kind modified Bessel function of zeroth order and

$$A_{mn} = 2\rho U \frac{1 - \cos(k_n \mu)}{k_n} \quad (3.36)$$

To calculate the pressure impulse for a slamming wave on a vertical cylinder the following equation is used:

$$\frac{P}{\rho U H} \left( \frac{r}{H}, \theta, \frac{z}{H} \right) = f \left( \frac{b}{H}, \mu, \frac{a}{b}, \theta_{max} \right) \quad (3.37)$$

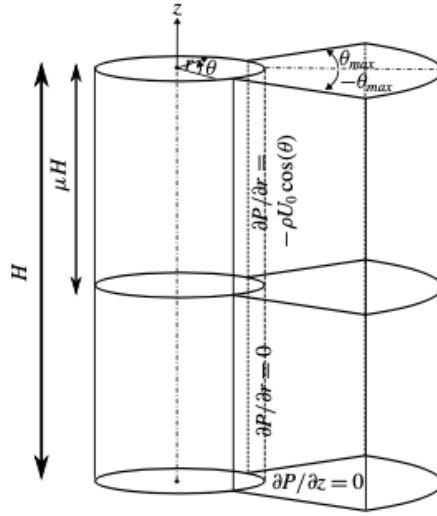


Figure 3.10: Definition sketch for wedge-shaped 3D impact on a vertical cylinder.  
(Ghadirian & Bredmose, 2019)

Where:

$\frac{b}{H}$  – Relative length of the impacting wave

$\mu$  – Relative height of the impacting zone

$\frac{a}{b}$  – Relative inner radius

$\theta_{max}$  – Azimuthal angle limit

For the vertical cylinder the fluid in the azimuthal direction is wedge shaped, as shown in the figure above the limits are set to  $-\theta_{max} \leq \theta \leq \theta_{max}$ . The fluid is in contact with the cylinder in the lower part  $-H \leq z \leq -\mu H$ , while the impact force on the cylinder is acting on the upper part  $-\mu H \leq z \leq 0$  with a velocity of  $U \cos(\theta)$  working in negative radial direction.

The Laplace equation is used to calculate the impact on the cylinder with azimuth limits in the cylindrical coordinate system as follows:

$$P = \sum_{m=1}^{\infty} \sum_{n=1}^{\infty} \left( A_{mn} \cos\left(\frac{L_m \theta}{\theta_{max}}\right) \sin\left(k_n \frac{z}{H}\right) \frac{I_{qm}\left(k_n \frac{r}{H}\right) + \alpha_{mn} K_{qm}\left(k_n \frac{r}{H}\right)}{\partial_r \left( I_{qm}\left(k_n \frac{r}{H}\right) + \alpha_{mn} K_{qm}\left(k_n \frac{r}{H}\right) \right)_{r=a}} \right) \quad (3.38)$$



Where  $L_m = (m - 1/2)\pi$ ,  $k_n = (n - 1/2)\pi$  and  $q_m = L_m/\theta_{max}$  is the order of the Bessel functions. Further  $\alpha_{mn}$  is chosen such that  $P = 0$  at  $r = b$ ,

$$\alpha_{mn} = \frac{-I_{qm}\left(k_n \frac{b}{H}\right)}{K_{qm}\left(k_n \frac{b}{H}\right)} \quad (3.39)$$

And,

$$A_{mn} = \frac{2\rho U}{\theta_{max}} \frac{1 - \cos(k_n \mu)}{k_n} \int_{-\theta_{max}}^{\theta_{max}} \cos(\theta) \cos\left(\frac{L_m \theta}{\theta_{max}}\right) d\theta dz \quad (3.40)$$

## 4 Results and Analysis

### 4.1 MATLAB Results

This section presents the analysis of the pressure impulse model. The mathematical problem related to the pressure impulse model was executed using MATLAB, with the intention of reproducing the same results as the ones in Ghadirian & Bredmose (2019). The MATLAB m-file were written as an equation with boundary conditions, with the intention of producing the converged solution with all boundary conditions satisfied. The results achieved are in great agreement with the previous studies. In order to achieve the best mathematical guess on calculating wave load problems, a mathematical technique needs to be decided. The issue must be identified, numerically demonstrated, and solved using software. There are considerations that must be taken when deciding on the most suitable techniques for solving the issues which are performance, accuracy and the computational limit required. The computational model results from the numerical problems that consider the limits and administering conditions. Discretization is the main difference between these strategies.

The reliance on the length of the wave affected  $b/H$  is seen in figure 4.2 for  $a/H = 0.1$ ,  $\mu = 0.5$ ,  $\theta = 0$  and  $\theta_{\max} = \pi/4$ . The increasing pressure impulse grows in all heights as  $b/H$  increases up to 0.35 and then stays unaltered. This suggest that the expansion of  $b/H$  shows an asymptotic behavior. Cooker & Peregrine (1995) observed the same asymptotic conduct for the 2D plate flat case. The impact height reliance is investigated in figure 4.1. The values of  $a/H$ ,  $\mu$  and  $\theta_{\max}$  are the same as in figure 4.3 and a width of  $b/H = 0.3$  is utilized. The peak of the pressure impulse drops as expected with increase of  $\mu$ , and results in pressure impulse expansion. The results from this figure are consistent with the ones in Cooker & Peregrine (1995). Figure 4.1 examines the variation for different values of the inner radius  $a/b$ , for  $b/H = 0.3$ ,  $\mu = 0.5$  and  $\theta_{\max} = \pi/4$ . The pressure impulse increases as the inner radius increases until  $a/b = 0.5$ . For the case with axisymmetric impact the pressure impulse decreases similarly for values of the inner radius larger than  $a/b = 0.67$ . The pressure impulse increases when the area that absorbs the incident momentum increases due to increased radius. The volume of fluid that influences the cylinder decreases simultaneously. The greatest pressure impulse is generated inside the interval  $0.5 < a/b < 0.7$ . The pressure impulse increases when the width of the area increases, due to the expansion of the volume of fluid  $V = (b^2 - a^2)\theta_{\max}\mu H$  as  $\theta_{\max}$  increases. When the azimuthal angle limit increases the pressure impulse also rises until the limit of the azimuthal point is reached at  $\theta_{\max} = \pi/2$ .

The results obtained using MATLAB were reproduced using a MATLAB script provided by Assoc. Prof. Charlotte Obhrai, to validate the results presented by Ghadirian & Bredmose (2019). The script provided were written for a vertical circular cylinder, with the parameters  $\mu = 0.5$ ,  $\frac{b}{H} = 1$  and  $\frac{W}{H} = 0.5$ . The results from the MATLAB script as shown below is in excellent agreement with the results from Ghadirian & Bredmose (2019).

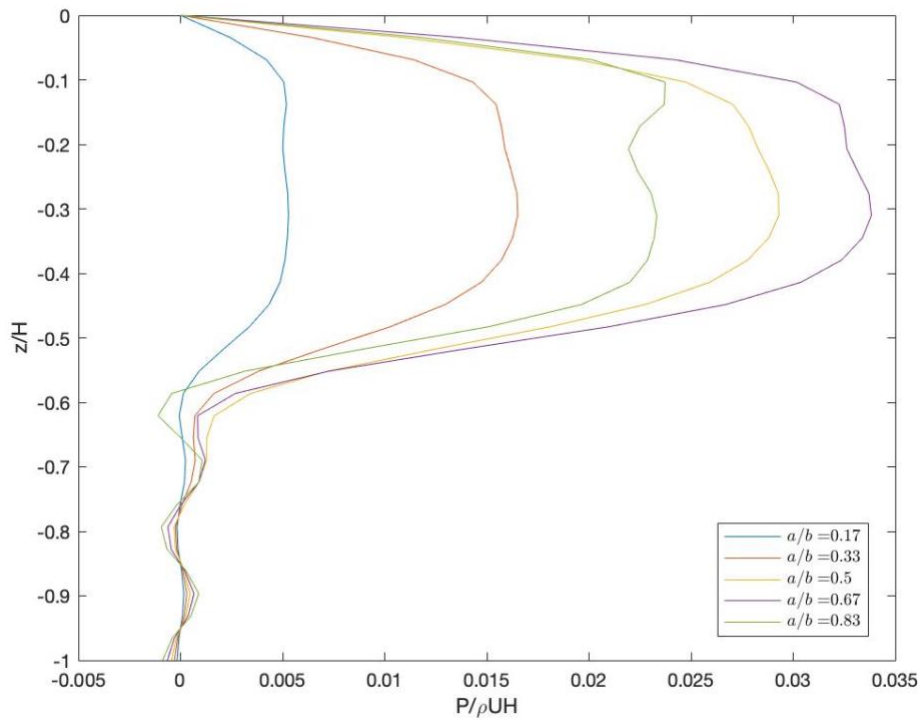


Figure 4.1: Dimensionless pressure impulse on the cylinder plotted as a function of  $z/H$ , at  $\theta = 0$ , for several values of  $a/b$

The relative inner radius,  $a/b$  is investigated in figure 4.1 where  $\theta_{max} = \pi/4$ ,  $\mu = 0.5$  and  $b/H = 0.3$ . When the relative inner radius is increasing up to 0.5, the pressure impulse also increases. The pressure impulse decreases for values of the inner radius larger than 0.67. As shown in this simulation, the radius is increasing, so when the value,  $a$ , increases the area on the cylinder that is impacted by the wave also increases. This results in an increasing pressure impulse. At the same time the volume of the impacting fluid decreases when the radius of the cylinder increases, this results in reaching a maximum in pressure impulse within the interval  $0.5 < a/b < 0.7$ .

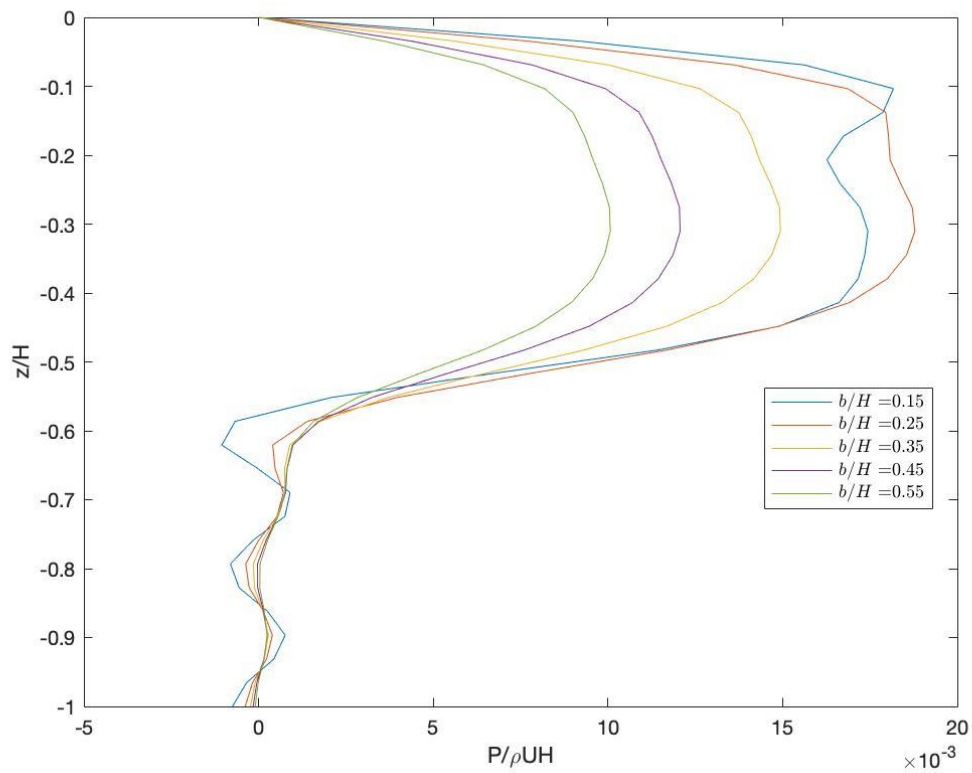


Figure 4.2: Dimensionless pressure impulse on the inner cylinder, at  $\theta = 0$ , plotted as a function of  $z/H$  for several values of  $b/H$

In figure 4.2 the relative length of the impacting wave  $b/H$  is investigated where  $\theta_{max} = \pi/4$ ,  $\theta = 0$ ,  $\mu = 0.5$  and  $a/H = 0.1$ . The pressure impulse increases in all dimensions and stays unchanged afterwards for  $b/H$  increasing up to 0.35. This shows that the behavior when increasing  $b/H$  is asymptotic.

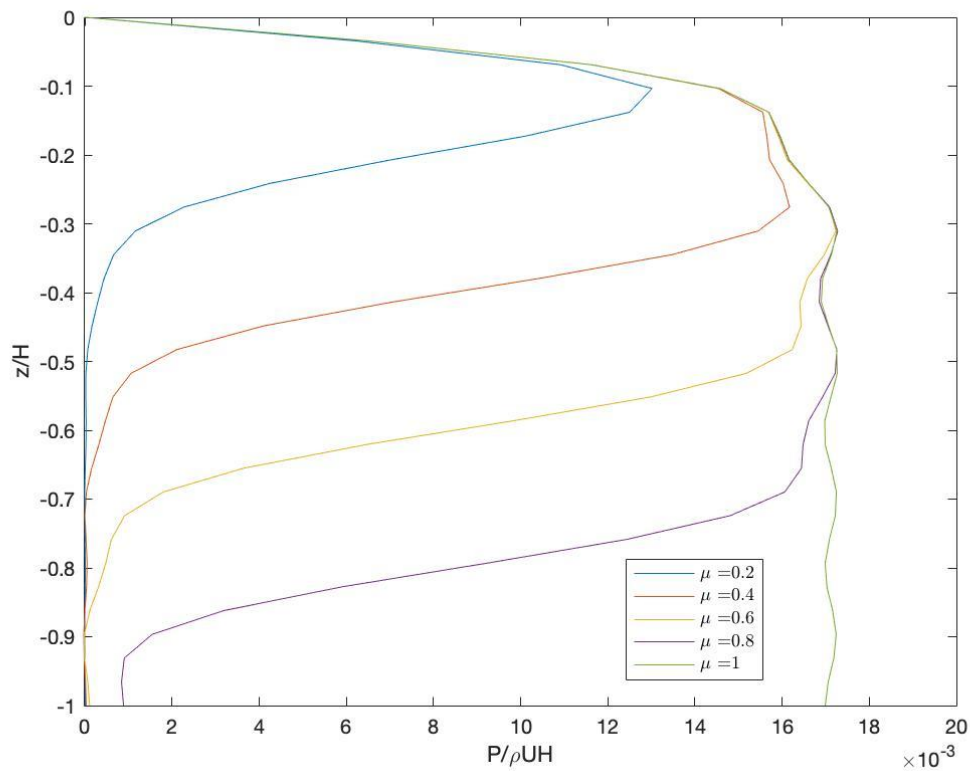


Figure 4.3: Dimensionless pressure impulse on the inner cylinder, at  $\theta = 0$ , plotted as a function of  $z/H$  for several values of  $\mu$

The height of the impact zone is investigated in figure 4.3, where  $\theta_{max} = \pi/4$ ,  $\mu = 0.5$ ,  $a/H = 0.1$  and  $b/H = 0.3$ . When the relative height of the impacting zone increases, the peak of the pressure impulse drops down and results in increasing pressure impulse.

The acting force impulse increases when the azimuthal limit grows up until  $\pi/2$  where it peaks. The change in the pressure impulse with regard to  $\theta_{max}$  is homogeneous and robust. This parameter can be used to perform calibration for similar comparable cases. The models total pressure impulse can be analyzed up to the already established models of Goda et al. (1966) and Wienke & Oumeraci (2005). These models are respectively around 190% and 100% overestimated due to the predicted most extreme force and the time frame, which has been validated less significantly in prior studies (Ghadirian & Bredmose, 2019).

The model was validated against an actual wave impact. It takes into account the phase and direction of the selected waves sea state which is for a cylinder of a diameter of 7 m at a water depth of 33 m, with wave period  $T_p = 12$  s and significant wave height  $H_s = 9.5$  m. Computational fluid dynamics (CFD) results at scale 1 : 50 for this impact were presented by Ghadirian, Bredmose & Dixen (2016). Figure 4.4 shows the CFD model with the black line being the inline force without the slamming impulse, and the blue shaded region is the effect of the integrated impulse pressure on a cylinder structure. The time is normalized by  $R/C$ , and the force is normalized by  $\rho C^2 R^2$ , where  $R$  is the radius of the circular cylinder,  $\rho$  is the water density and  $C$  is the wave celerity. To isolate the contribution of the non-impacting parts of the wave to the force impulse, the pressure on the cylinder was taken out of the equation for all CFD results before the impact. The CFD model shows the impact pressure integrated over the duration of the impact (Ghadirian & Bredmose, 2019).

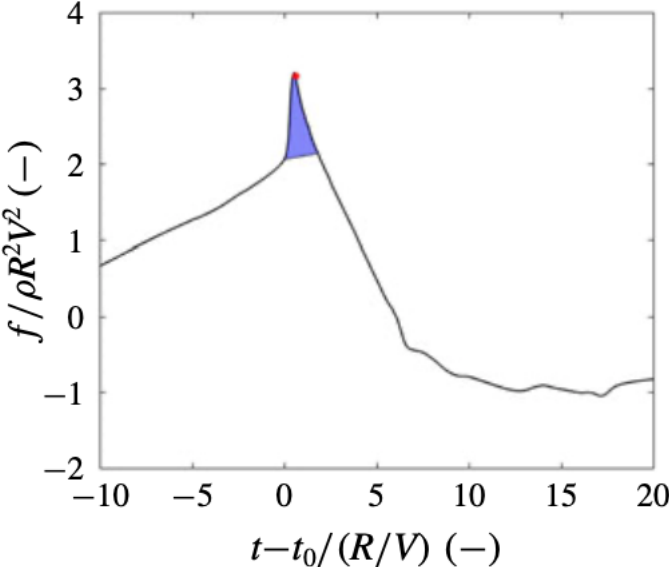


Figure 4.4: Inline force time series with and without the slamming effect. (Ghadirian & Bredmose, 2019)

From the realistic sea state mentioned above, the pressure impulse model and the parameters are chosen to best compute the impulse pressure for the realistic sea state showed in figure 4.5. Here  $\mu$  is determine based on the height of the breaking wave. Further  $b$  is selected as the length from center of the cylinder to the rear of the wave crest at still-water level. Consequently  $\mu = 0.12$ ,  $a/b = 0.13$ ,  $b/H = 0.64$ ,  $a/H = 0.0832$  and  $\theta_{\max} = \pi/4$ . The limits for the computed pressure impulse are  $z/H_{\min} = -1$  and  $z/H_{\max} = 0$ , which is a description of the impacting zone,  $\theta_{\min} = 0$  and  $\theta_{\max} = 0$ . The number of discretized points,  $N_{\text{points}} = 331$ , which is the number of points the pressure impulse is computed over the impacting height. To compare the impact force from the pressure impulse model to the DNVGL and IEC models, the force impulse for each needs to be obtained. The force impulse from the pressure impulse model is determined by first de-normalizing the pressure impulse with  $\rho UH$ , where density of water ( $\rho$ ) and water depth ( $H$ ) is known, and impact velocity is assumed to be  $U = \omega H$  (Almeida & Hofland, 2020). Then, the pressure impulse is integrated over the height of the impact zone to obtain the force impulse. The force impulse,  $I_{\text{imp}}$ , is estimated to be  $I_{\text{imp}} = 141069$  Ns for the pressure impulse model.

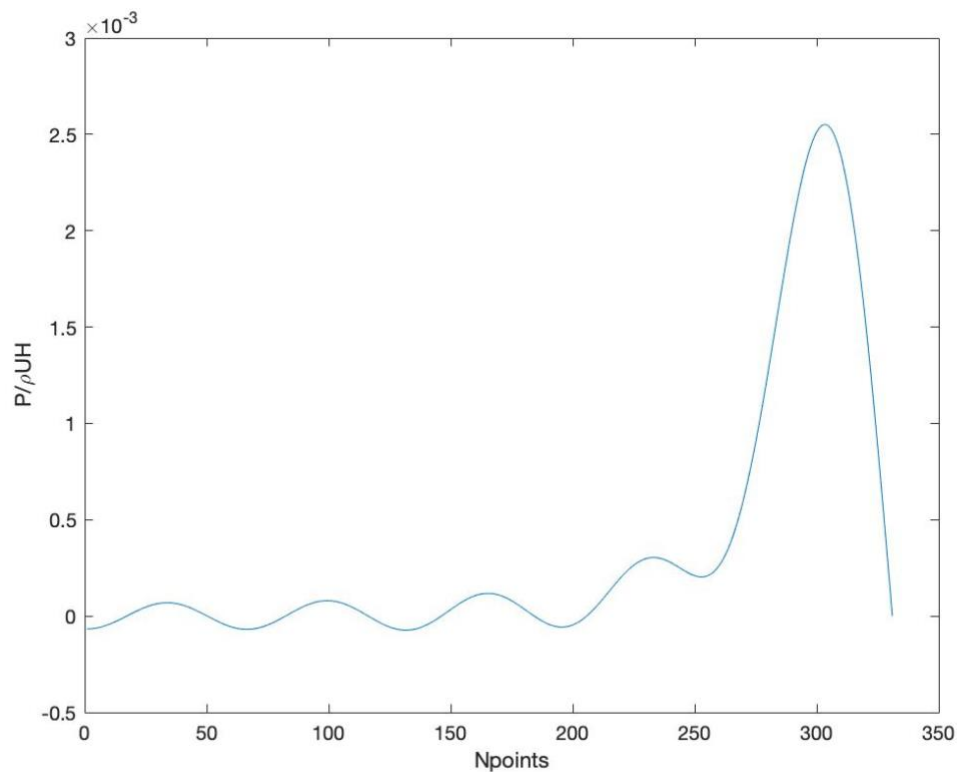


Figure 4.5 Dimensionless pressure impulse at every discretized point for the realistic sea state

## 4.2 DNVGL & IEC Standards

The sea state Ghadirian & Bredmose (2019) applied to validate the pressure impulse model against realistic wave impact was  $H_s = 9.5$  m and  $T_p = 12$  s, with a water depth of 33 m and a cylinder diameter of 7 m. The drag and inertia coefficients were also chosen to best compare the results from pressure impulse and realistic wave impact, in this case the drag coefficient,  $C_D = 1.0$ , and inertia coefficient,  $C_M = 1.79$ . The wave celerity, the breaking wave velocity and the slam coefficient were not mentioned in Ghadirian & Bredmose (2019) description of the sea state, other than mentions of von Karman and Wagner`s theories with coefficients of  $\pi$  and  $2\pi$ . The drag, inertia and impact forces have been estimated numerically by using Excel, and the particular values for cylinder diameter, wave height, wave period and water depth. The wavelength is determined to  $\lambda = 182.1$  m, the wave number  $k = 0.0345$  rad/m and the angular wave frequency  $\omega = 0.524$  rad/s.

### 4.2.1 Drag and Inertia Force Time Histories

Based on the guidelines provided in IEC and DNVGL standards described in chapter 3.2, the drag and inertia force are determined for the relevant sea state with the use of Morison equation. The total force from the Morison equation is obtained by integrating the force acting over the height of the structure.

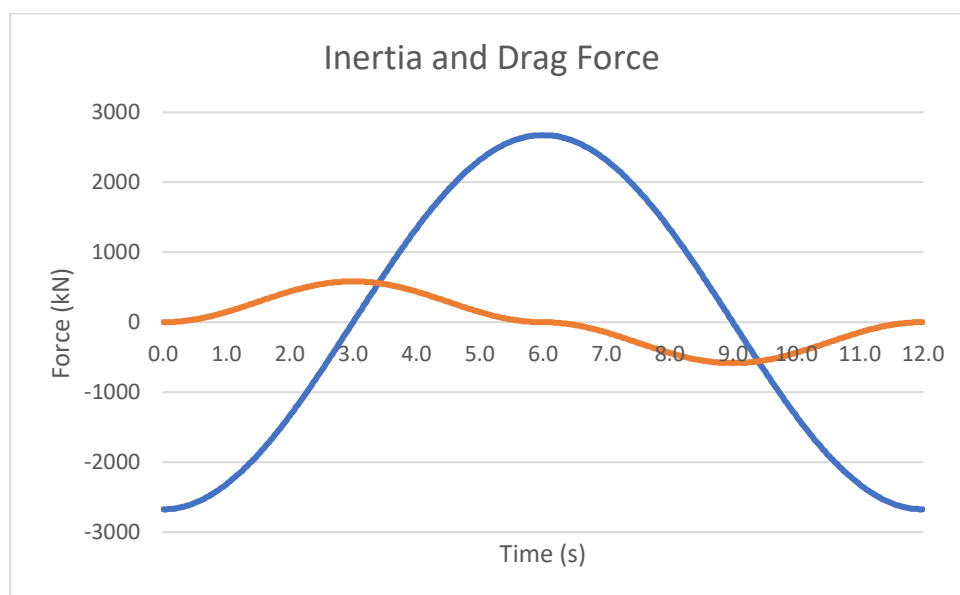


Figure 4.6 Time series for the drag and inertia force.



In figure 4.6 the time history of the drag and inertia force are shown, with the maximum and minimum drag force occurring when inertia force is equal to zero and the maximum inertia force occurring when drag force is equal to zero. The inertia force is dominant compared to the drag force but not neglectable as seen if figure 4.7, and the difference is smaller due to the decision of reducing the inertia coefficient from  $C_M = 2.0$  to  $C_M = 1.79$  according to Ghadirian & Bredmose (2019). The impact force is added to the Morrison force in figure 4.8 and 4.9 for the two impact models presented in figure 4.11 and 4.12. The impact duration for the two models is  $T_{IEC} = 0.08$  s and  $T_{DNVGL} = 0.4$  s, which is easily seen as the short duration, high impact force in both models.

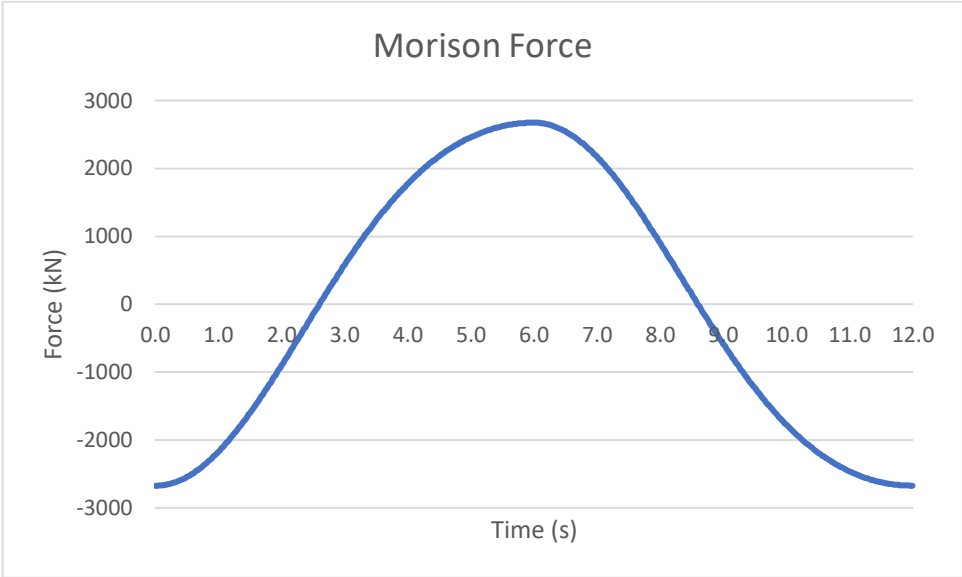


Figure 4.7 Time series of the combined drag and inertia force (Morrison force).

The time history of the inline force in figure 4.4 is more drag dominated than seen in the calculations for the Morrison force, although the time histories are not necessarily comparable, the impulse pressure from the CFD model for the given sea state can be compared to the impulse pressure determined with the IEC and DNVGL models.

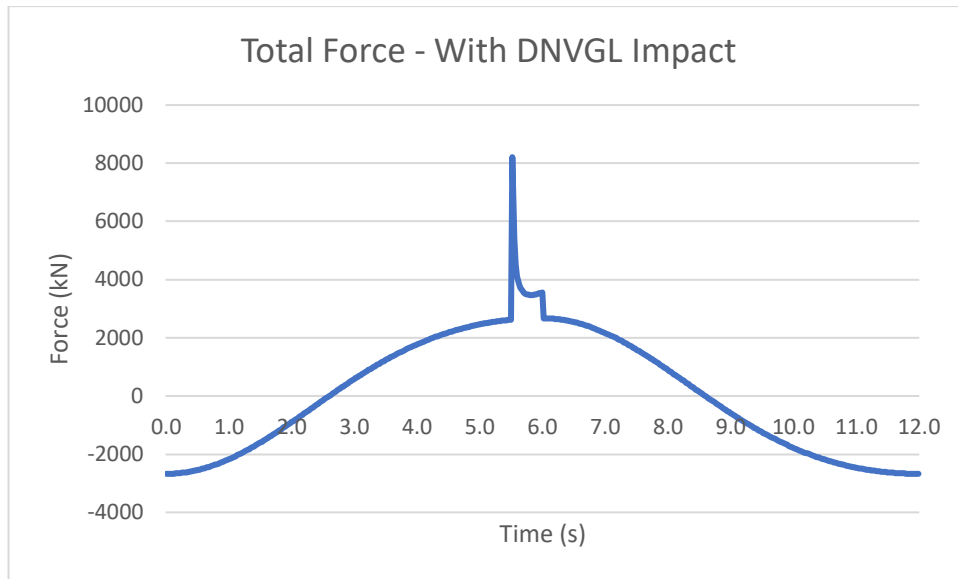


Figure 4.8 Total force time history with DNVGL impact force

The IEC model estimates a higher impact force than the DNVGL model due to a higher slamming coefficient, and the duration of impact is significantly shorter. The impact force is added to the Morrison equation during its time of impact, and the singularity of the impact force at the start implies that the force increases instantaneously and therefore results in the discontinuity of the force time series.

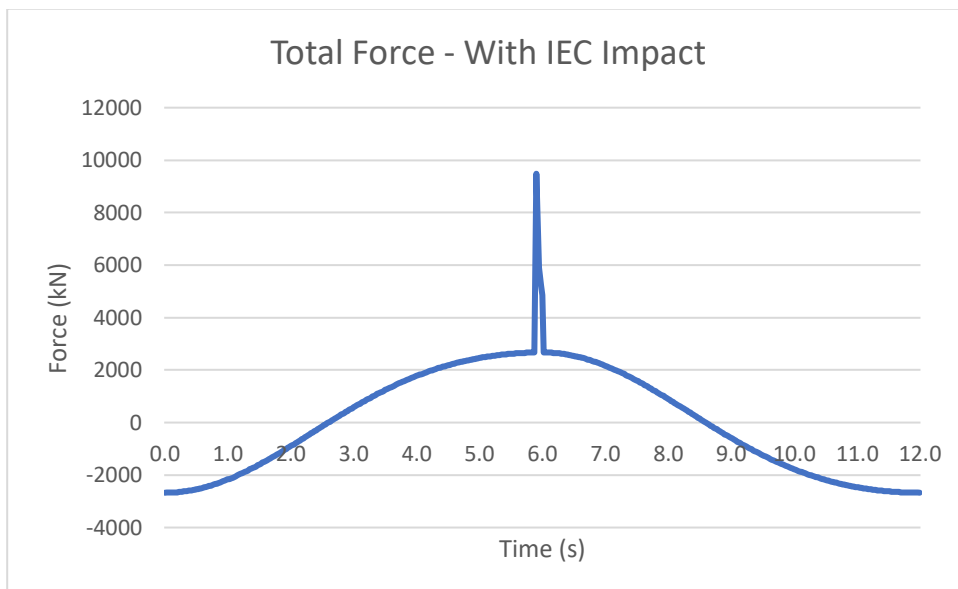


Figure 4.9 Total force time history with IEC impact force

#### 4.2.2 Slam Coefficients Time Histories

The slam coefficient is determined using guidelines presented in IEC 61400-3 (2009) and DNVGL-RP-C205 (2017). Figure 4.10 plots the slam coefficients time histories for the two slam coefficient models. The shape of these slam coefficient time histories indicates that Wienke & Oumeraci's model has a higher maximum impulse over a shorter duration of time, and a step-by-step decrease of the coefficient due to different slam coefficient calculations for the first half and second half of the total duration of impact time. Campbell & Weynberg's model has a longer duration of impact and a gradual decrease of the coefficient, but lower maximum impulse due to a lower slamming coefficient at start of impact  $C_s(0) = 5.15$ , where Wienke & Oumeraci's coefficient at start of impact is  $C_s(0) = 2\pi$ . Common for these slam coefficients is that the rise time of the development at  $t = 0$  is infinitely short.

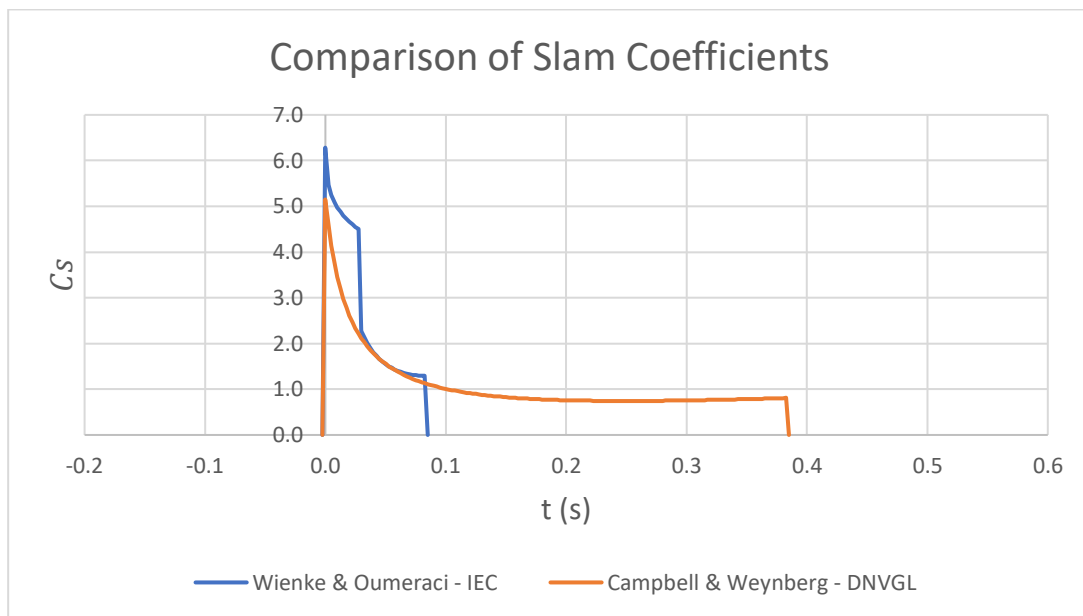


Figure 4.10 Comparison of slam coefficient time histories.

### 4.2.3 Impact Force Time Histories

The slam force is determined for the two coefficient models, where the force at impact varies due to the difference in duration of impact. The DNVGL model in figure 4.11 predicts a lower slam force at impact but has a higher post impact force due to a longer duration.

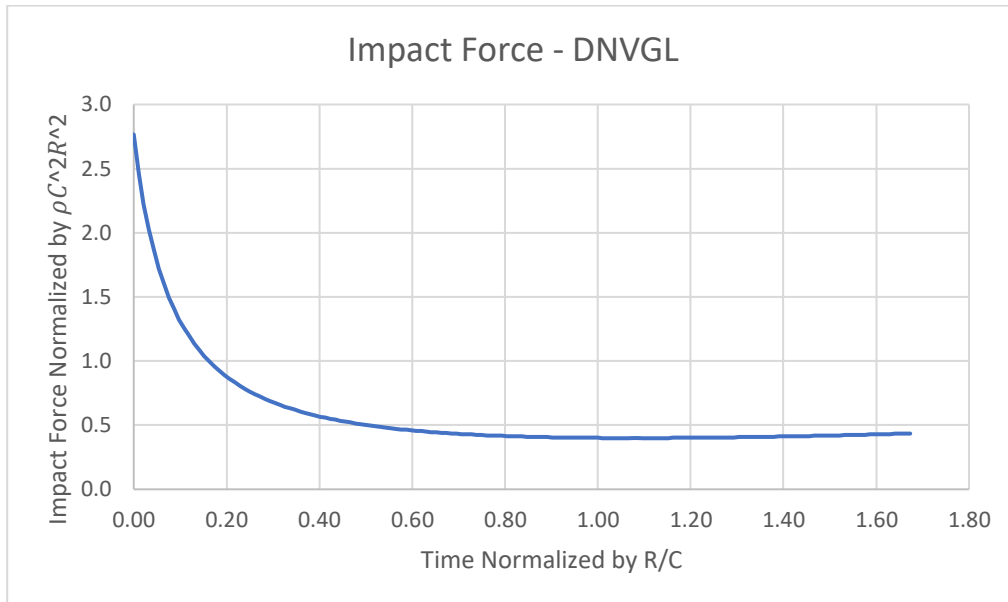
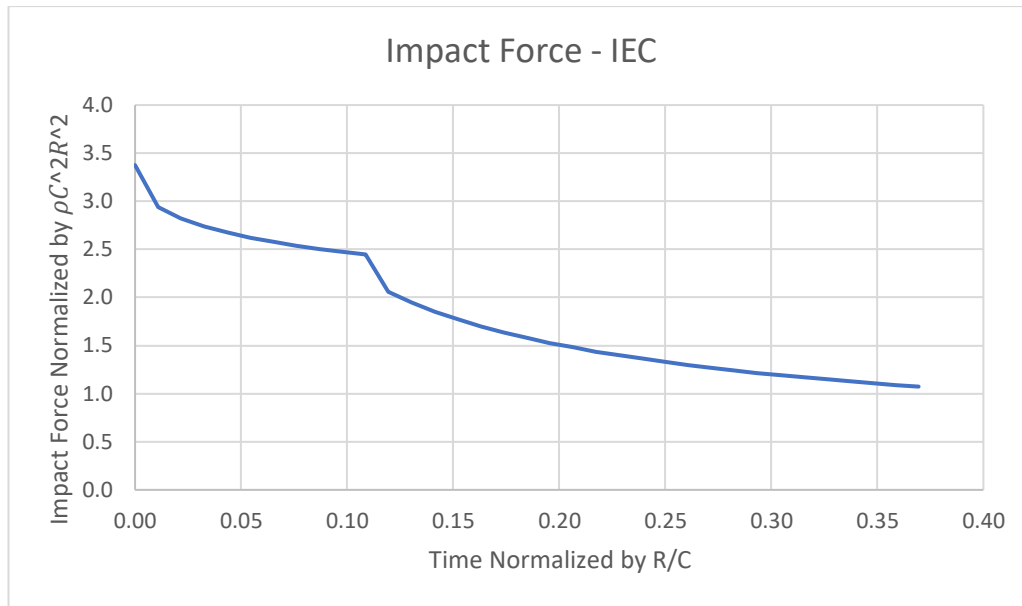


Figure 4.11 Time history of the normalized DNVGL impact force.

DNVGL-RP-C205 (2017) states that the impact height is 0.25 times the wave height at breaking ( $0.25 \cdot H_b$ ), and that the width is taken as a sector of 45 degrees. IEC 61400-3 (2009) states that the impact height is defined as curling factor times the maximum elevation of the free water surface ( $\eta_b \cdot \lambda$ ), and the width is taken as the radius of the cylinder. The difference in the impact area is not significant due to the similar values for both the height and the width of the two models.

The force impulse for the IEC and DNVGL models are defined by integrating the impact force from the breaking wave over the impulse duration for each model. Where the impact duration for the two models is  $T_{DNVGL} = 0.4$  s and  $T_{IEC} = 0.08$  s. The force impulse estimated for the DNVGL standard is  $I_{DNVGL} = 563371$  Ns and for the IEC standard is  $I_{DNVGL} = 424578$  Ns.



*Figure 4.12 Time history of the normalized IEC impact force.*

The force impulse obtained from the IEC standard with Wienke & Oumeraci`s (2005) model overpredicts the force impulse by 201 % compared to the pressure impulse model. This value is similar to the overprediction estimated by Ghadirian & Bredmose (2019), which is approximately 190 % for the Wienke & Oumeraci`s (2005) model. The force impulse determined from the DNVGL standard with Campbell & Weynberg`s (1980) model is 299 % overpredicted compared to the pressure impulse model.

## 5 Discussion

The results obtained with the MATLAB script provided is in excellent agreement with the results obtained by Ghadrian & Bredmose (2019), which indicates that the model is effective for calculating real impact of waves. Also, the impact of waves on a bottom fixed monopile is determined with the guidelines provided in DNVGL-RP-C205 (2017) and IEC 61400-3 (2009). The impact force computed from Wienke & Oumeraci (2005) and Campbell & Weynberg (1980) model shows the behavior of the impact force and the impact duration of the breaking wave, which has a similar behavior as the CFD models force time series in figure 4.4. The force impulse based on the IEC and DNVGL models is estimated to be 201 % and 299 % overpredicted respectively compared to the pressure impulse model. As shown, the results obtained in this study shows that the recommended standards for design requirements are overpredicting the determined impulse force compared to the pressure impulse model. Future work may compare different sea states to the pressure impulse model, to gain insight and knowledge for a more accurate comparison of the different methods.

## 6 Conclusion

In this project the breaking wave loads has been determined using the pressure impulse model for an idealized wave on a cylinder with azimuth limits for a specific sea state. A provided MATLAB model was applied to calculate the pressure impulse on the cylinder by implementing some parameters for the sea state of interest. The initial MATLAB results is validated against the CFD results by Ghadirian & Bredmose (2019) showing excellent agreement. The force impulse, drag force and inertia force has also been determined by using recommended guidelines from DNVGL and IEC. The impulse force for the different impact models has been analyzed and compared to establish the difference in magnitude of the impulse forces, and the guidelines presented in IEC and DNVGL overpredicts the impulse force compared to the pressure impulse model. These models are excellent tools to provide predictions of the Ultimate Lime State (ULS) wave loads on a bottom fixed monopile with some of these predictions being more conservative.

## References

- Almeida, E., & Hofland, B. (2020). Validation of pressure-impulse theory for standing wave impact loading on vertical hydraulic structures with short overhangs. *Coastal Engineering*, 159, 103702.
- Chella, A.M., Bihs, H., Myrhaug, D., Muskulus, M., (2016). Breaking solitary waves and breaking wave forces on a vertically mounted slender cylinder over an impermeable sloping seabed. *J. Ocean Eng. Mar. Energy*, 1–19.
- Chella, M. A., Tørum, A., & Myrhaug, D. (2012). An Overview of Wave Impact Forces on Offshore Wind Turbine Substructures. *Energy Procedia*, 20, 217–226.
- Cointe, R. & Armand, J.-L. (1987). Hydrodynamic impact analysis of a cylinder. *Trans ASME J. Offshore Mech. Arctic Engng* 109 (3), 237–243.
- Cooker, M. J. & Peregrine, H. (1995). Pressure-Impulse Theory for Liquid Impact Problems. *J. Fluid Mech.* 297, 193–214.
- DNV-OS-J101. (2014). Design of offshore wind turbine structures.
- DNVGL-RP-C205. (2017). Environmental conditions and environmental loads.
- DNVGL-ST-0437. (2006). Loads and site conditions for wind turbines.
- European Commission. (2020). Stepping up Europe`s 2030 climate ambition – Investing in climate-neutral future for the benefit of our people. 562 Final.
- Ghadirian, A. and H. Bredmose (2019). "Pressure impulse theory for a slamming wave on a vertical circular cylinder." *Journal of Fluid Mechanics. Fluid Mech.* 867.
- Goda, Y., Haranaka, S. & Kitahata, M. (1966). Study On Impulsive Breaking Wave Forces on Piles. Tech. Rep.

International Electrotechnical Commission (IEC), (2009). IEC 61400-3: Wind Turbines Part 3: Design Requirements for Offshore Wind Turbines, 1st Edition.

Leite O.B, (2015). “Review of Design Procedures for Monopile Offshore Wind Structures,” University of Porto, Porto.

Mokrani, C., Abadie, S., Grilli, S., and Zibouche, K., (2010). Numerical Simulation of The Impact of a Plunging Breaker on a Vertical Structure and Subsequent over Topping Event Using a Navier-Stokes VOF Model. In Proceedings of the Twentieth (2010) International Offshore and Polar Engineering Conference, pages 729 736, Beijing, China.

Pierella, F., Ghadirian, A., & Bredmose, H. (2019). Extreme Wave Loads on Monopile Substructures: Precomputed Kinematics Coupled With the Pressure Impulse Slamming Load Model. *ASME 2019 2nd International Offshore Wind Technical Conference*, V001T01A011.

Tanimoto, K., Takahashi, S., Kaneko, T., Shiota, K., (1986). Impulsive breaking wave forces on an inclined pile exerted by random waves. Proceedings of the 20th International Conference on Coastal Engineering, vol. 3, pp. 2288 2302.

Wienke, J. & Oumeraci, H. (2005). Breaking wave impact force on a vertical and inclined slender pile – Theoretical and large-scale model investigations. *Coast. Engng* 52 (5), 435–462.

WindEurope & ETIPWind. (2021). Getting fit for 55 and set for 2050 – Electrifying Europe with wind energy.



## Appendix

```
function [Pxyz, P] = PressureImpulseFunction(thetamin, thetamax, zHmin, zHmax, ... mu,
aoverH, boverH, theta_max, M, N, Npoints)
%%
rhoUH = 1; % one because I intend to evaluate P/rhoUH
mlarge = M;
nlarge = N;
%%
rHmin = aoverH;
rHmax = boverH;
zoverH = linspace(zHmin, zHmax, Npoints)'; % limits for z/H
% theta = linspace(thetamin, thetamax, Npoints)'; % limits for y/W
% roverH = linspace(rHmin, rHmax, Npoints)'; % limits for x/H
thetaLIM = linspace(thetamin, thetamax, Npoints)'; % limits for y/W
roverHLIM = linspace(rHmin, rHmax, Npoints)';

% Initializes P(x,y,z)
Pxyz = zeros(size(Npoints, 1));
for tt = 1: numel(roverHLIM)

    roverH = roverHLIM(tt) ;
    fprintf('\n roverH = %g \t', roverH)

for ttt = 1: numel(thetaLIM)

    theta = thetaLIM(ttt) ;
    fprintf('theta = %g \n', theta)

syms roverH_ t heta_

for m = 1: mlarge
% fprintf('m = %d /t', m)
```

```
For n= 1: nlarge
```

```
L_m = (m - 1/2)*pi ;
```

```
k_n = (n - 1/2)*pi ;
```

```
qm = L_m/theta_max ;
```

```
% Equation 2.13
```

```
DZ = diff(zoverH,1); dz = DZ(1);
```

```
A_mn = 2*rhoUH./theta_max*(1 - cos(k_n *mu))/k_n * ... (double(integral(@(theta_)  
cos(theta_).*cos(L_m.*theta_/theta_max), -theta_max, theta_max))*dz ;
```

```
% (double(vpintegral(cos(theta_).*cos(L_m.*theta_/theta_max), [-  
theta_maxtheta_max]))) *dz ;
```

```
% Equation 2.12
```

```
alpha_mn = - besseli(qm,k_n.*boverH)./besselk(qm, k_n.*boverH) ;
```

```
% Equation 2.11
```

```
P_instant = (A_mn .* cos(L_m .*theta./theta_max).*sin(k_n.*zoverH) .*...
```

```
(besseli(qm,k_n.*roverH) + alpha_mn.*besselk(qm,k_n.*roverH))...
```

```
./ double(subs(diff(besseli(qm,k_n.*roverH_) + alpha_mn.*besselk(qm,k_n.*roverH_),  
roverH_),roverH_, aoverH)));
```

```
Pxyz = Pxyz + (P_instant);
```

```
% % %
```

```
% % % %
```

```
end
```

```
if n == nlarge
```

```
fprintf('n = %d \t', n)
```

```
end
```

```
m =mlarge;
```

```
if m == mlarge
```

```
fprintf('m = %d \t', m) end
```

```
end
```

```
if ~any(diff(thetaLIM)) break
```

```
end
```

```

end end
% get Vector P
P = Pxyz;
% end

%% Figure 9 (a)
% prepares and clears all existing variable(s) in workspace as well as command window
clear,clc
close all % close all opened figures
%%
% Values to be varied: M and N
M = 10;
N = 10;
Npoints = 30; % Number of discretized points to evaluate
theta_max = pi/4;
% aoverb = 0.5;
aoverH = 0.1;
% Limits
thetamin = 0; thetamax = 0;
zHmin = -1; zHmax = 0;
% other parameters
mu = 0.5;

%% Figure 9 (a)
% Dimensionless pressure impulse on the inner cylinder,
% at  $\theta = 0$ , plotted as a function of  $z/H$  for several values of  $b/H$ .
boverH = [0.15 0.25 0.35 0.45 0.55]';
aoverb = aoverH ./boverH;
for i = 1: length(aoverb)
[Pxyz, P] = PressureImpulseFunction(thetamin, thetamax,zHmin,zHmax,... mu, aoverH,
boverH(i), theta_max, M, N, Npoints);
Pxyz_Variant{i} = Pxyz; % MATRIX P
P_2{i} = P;
i=i end

```

```

%%
zoverH = linspace(zHmin, zHmax, Npoints)'; % limits for y/W figure(1)
for i = 1: length(aoverb)
plot(P_2{i},zoverH)
legendcell2{i} = strcat('$b/H$ = ',num2str(boverH(i)));
hold on
end
hold off
ylabel('z/H')
xlabel('P/\rhoUH')
h1 = legend(llegendcell2{1:end});
set(h1, 'Interpreter', 'latex','Location','Best');

%% Figure 9 (b)
% prepares and clears all existing variable(s) in workspace as well as command window
clear,clc
% close all % close all opened figures
%%
% Values to be varied: M and N
M = 10;
N = 10;
Npoints = 30; % Number of discretized points to evaluate
theta_max = pi/4;
aoverb = 0.5;
aoverH = 0.1;
boverH = 0.3;
% Limits
thetamin = 0;
zHmin = -1;
% other parameters
mu = 0.5;

```

```

%% Figure 9 (b)
% Dimensionless pressure impulse on the inner cylinder, at  $\theta = 0$ ,
% plotted as a function of  $z/H$  for several values of  $\mu$ .
thetamax = 0; zHmax = 0;
% update
mu = [0.2 0.4 0.6 0.8 1.0];
boverH = 0.3;
aoverH = 0.1;
% aoverH = aoverb .* boverH ;
for i = 1: length(mu)
[Pxyz, P] = PressureImpulseFunction(thetamin, thetamax,zHmin,zHmax,... mu(i), aoverH,
boverH, theta_max, M, N, Npoints);
Pxyz_Variant{i} = Pxyz; % MATRIX P
P_3{i} = P;
end
zoverH = linspace(zHmin, zHmax, Npoints)'; % limits for y/W figure(2)
for i = 1: length(mu)
plot(P_3{i}, zoverH)
legendcell2{i} = strcat('\mu$ = ',num2str(mu(i))); hold on
end
hold off
xlabel('P\rhoUH')
ylabel('z/H')
% legendcell2 = strcat('$w/H$ = ',string(num2cell(WoverH))); h1 =
legend({legendcell2{1:end}});
set(h1, 'Interpreter', 'latex', 'Location','Best');

%% Figure 10 (a)
% prepares and clears all existing variable(s) in workspace as well as command window
clear,clc
% close all % close all opened figures
%%
% Values to be varied: M and N
M = 10;

```

```

N = 10;
Npoints = 30; % Number of discretized points to evaluate
theta_max = pi/4;
% aoverb = 0.5;
aoverH = 0.1;
% Limits
thetamin = 0; thetamax = 0;
zHmin = -1; zHmax = 0;

%% Figure 10(a)
% other parameters:
aoverb = [0.17 0.33 0.50 0.67 0.83];
boverH = 0.3;
mu = 0.5;
aoverH = aoverb .* boverH ;
for i = 1: length(aoverb)
[Pxyz, P] = PressureImpulseFunction(thetamin, thetamax,zHmin,zHmax,... mu, aoverH(i),
boverH, theta_max, M, N, Npoints);
Pxyz_Variant{i} = Pxyz; % MATRIX P
P_4{i} = P;
end
zoverH = linspace(zHmin, zHmax, Npoints)'; % limits for y/W figure(3)
for i = 1: length(aoverb)
plot(P_4{i},zoverH)
lengendcell2{i} = strcat('$a/b$ = ',num2str(aoverb(i)));
hold on
end
hold off
ylabel('z/H')
xlabel('P/\rho UH')
h1 = legend(lengendcell2{1:end});
set(h1, 'Interpreter', 'latex','Location','Best');
%

```